International Journal of Fatigue 216 (2027) 110065

Contents lists available at ScienceDirect

International Journal of Fatigue

journal homepage: www.elsevier.com/locate/ijfatigue

Influence of concrete composition on fatigue life: Machine learning-based prediction of the number of cycles to failure

Sören Voß [a,*], Silke Scheerer [a], Raúl Enrique Beltrán Gutiérrez [a], Thorsten Betz [b], Chongjie Kang [a,c], Steffen Marx [a,c]

[a] Institute of Concrete Structures, Technische Universität Dresden, Dresden, Germany
[b] Max Bögl Wind AG, Neumarkt in der Oberpfalz, Germany
[c] Cluster of Excellence CARE, TU Dresden and RWTH Aachen, Germany

ARTICLE INFO

Keywords:
Fatigue
Concrete composition
Machine learning
Fatigue life
Compressive fatigue loading
Number of cycles to failure

ABSTRACT

Current fatigue design regulations employ conservative safety factors and do not account for the influence of concrete composition. Experimental evidence indicates that concretes with similar compressive strength but different compositions can exhibit considerably different fatigue life. Integrating concrete composition into fatigue design therefore has considerable potential to improve the accuracy of fatigue life predictions while maintaining structural safety and facilitating more resource-efficient concrete structures. Against this background, systematic fatigue tests under cyclic compressive loading were conducted on 18 high-strength concretes with varying compositions but comparable compressive strengths, under identical test conditions. For each concrete, fatigue behavior was evaluated at a minimum of four stress levels, resulting in a total of 241 fatigue tests. First, correlation analyses were performed for 16 of the 18 concrete compositions to identify test- and composition-related variables governing fatigue life. While the cement and binder contents exhibited negative correlation coefficients of approximately -0.50, the use of limestone showed a positive correlation coefficient of 0.63. Subsequently, six machine learning models were implemented to predict the number of cycles to failure based on concrete composition. The results demonstrated that the investigated models were able to predict fatigue life with reasonable accuracy. Among the evaluated approaches, neural networks and ensemble-based methods achieved the highest prediction accuracy, with R^2 values exceeding 0.95 for the training data and 0.90 for the test data. The predictions were validated using two additional concrete compositions withheld from model development, which showed good agreement between predicted and experimentally determined fatigue lives.

1. Introduction

The growing demand for environmentally sustainable electricity generation has increased the use of wind energy, highlighting the importance of fatigue-resistant wind turbine structures. Hybrid towers, consisting of precast, prestressed concrete elements in the lower section and a steel tower in the upper section, enable the construction of taller onshore wind turbines, including in regions with lower wind speeds [1,2]. Due to their slender design, wind turbines are exposed to high dynamic loads throughout their service life and must withstand more than 10^7 loading cycles [3–5]. Consequently, concrete fatigue can be a governing factor in the design of these structures. Also, fatigue is becoming increasingly relevant in bridge and civil engineering, as the higher compressive strength of modern concretes enables more slender cross sections and reduces structural dead load, thereby increasing the relative contribution of service loads [6,7].

However, in current design regulations, including Model Code 1990/2020 [8,9] and Eurocode 2 [10], substantially higher partial safety factors are applied to high- and ultra-high-strength concrete in fatigue design than in static design [11,12]. These increased safety factors are intended to account for the substantial scatter in the experimentally determined number of cycles to failure and are partly based on the assumption that higher-strength concrete is more susceptible to fatigue. However, this approach does not explicitly distinguish between the effects of test conditions and concrete composition on fatigue performance. In particular, current *S–N* curves generally do not account for the

* Corresponding author at: Institute of Concrete Structures, Technische Universität Dresden, Dresden 01062, Germany.
E-mail address: soeren.voss@tu-dresden.de (S. Voß).

https://doi.org/10.1016/j.ijfatigue.2026.110065
Received 15 September 2026; Received in revised form 21 October 2026; Accepted 28 October 2026
Available online 30 October 2026
0142-1123/© 2026 The Author(s). Published by Elsevier Ltd. This is an open access article under the CC BY license (http://creativecommons.org/licenses/by/4.0/).
Open access funding enabled and organized by Projekt DEAL.

influence of test conditions or concrete composition. As a result, this may lead to overly conservative designs for some concrete compositions and limit the efficient utilization of high-strength concrete.

In the literature, concrete fatigue has been extensively investigated, with numerous studies addressing the factors influencing its fatigue behavior and fatigue life [13–15]. However, comparatively limited research has focused specifically on the influence of concrete composition on fatigue life. Previous studies have indicated that the composition of concrete can affect its fatigue behavior and fatigue life [16]. Nevertheless, a clear and consistent relationship between concrete composition and fatigue life has yet to be established. Direct comparisons between published results are challenging because of the substantial variability in concrete compositions, specimen geometries, testing configurations, loading conditions, and other experimental parameters. Consequently, the available results do not permit a comprehensive and scientifically robust assessment of the influence of individual composition parameters on concrete fatigue life. Selected findings from previous studies are summarized below to illustrate the range of results reported in the literature. The selection is not intended to be exhaustive.

Type of coarse aggregate and material heterogeneity: When comparing basalt and granite aggregates, comparable numbers of cycles to failure were reported in [17]. In contrast, Oneschkow et al. [16] found that replacing basalt with granite had a beneficial effect on the fatigue life of high-strength concrete. This effect was attributed to the lower stiffness of granite, which resulted in a more homogeneous stress distribution within the concrete specimen. The magnitude of this effect depended on the compressive stress level and was also confirmed in [18]. Related investigations of stiffness distributions [19] showed that the lower stiffness of sandstone compared with quartzite and basalt resulted in a more uniform stiffness distribution within the concrete and, consequently, lower microcrack growth and stiffness degradation. The influence of material heterogeneity was also investigated in [20]. According to Oneschkow et al. [21], increasing aggregate size leads to a more heterogeneous stress distribution, while Li et al. [22] reported that a higher coarse aggregate content reduces fatigue life and increases brittleness.

Cement paste, fine-grained concrete, fine aggregates, and fibers: The interface between the cement paste and aggregate has long been considered a preferential location for microcrack initiation under fatigue loading. This was confirmed by CT scans in [23]. In [24], mortar was investigated under cyclic shear loading and exhibited higher numbers of cycles to failure than concrete at all investigated compressive stress levels, although the fatigue life of the mortar showed greater scatter. In contrast, Hordijk et al. [25] found no significant difference in fatigue behavior between concretes containing gravel and limestone powder. Silica fume and steel fibers are commonly used in high-strength concrete. The filling effect of silica fume can reduce the number and size of cracks in the interfacial transition zone and thereby improve the fatigue life of high-strength concrete and mortar [16,26]. Steel fibers can further improve cyclic performance by reinforcing the matrix, increasing stiffness, and bridging cracks. The combined use of silica fume and steel fibers was reported to increase the fatigue life of high-strength concrete by a factor of four compared with the reference composition [26].

Density and porosity: Higher porosity of the concrete or mortar microstructure, for example due to increased water content, has been associated with lower fatigue life [16,27,28]. The corresponding reduction in density has also been identified as an influencing factor [29].

Concrete strength: Numerous studies have reported a decrease in the number of cycles to failure with increasing concrete strength [30–36]. However, other studies have not confirmed this relationship or have found it to apply only under specific conditions [37]. For example, Basaldella et al. [38] reported higher numbers of cycles to failure for ultra-high-strength concrete than for high-strength concrete. Similar findings were reported in [12,39,40]. These results are not consistent with the assumptions underlying the partial safety factors specified in Model Code 1990/2020 [8,9] and Eurocode 2 [10]. Several studies have attributed the observed scatter in the number of cycles to failure to the variability in compressive strength [12,41,42].

Test conditions: Experimental conditions can also substantially affect the measured fatigue life. According to Basaldella et al. [43], the precision of the load application surfaces influences the scatter in the number of cycles to failure, although no significant effect on the mean fatigue life of high-strength concrete was observed. Loading frequency and temperature are further important factors [44–46]. At high frequencies, the associated increase in stress rate can increase the measured compressive strength and, consequently, the number of cycles to failure in short-duration tests. In long-duration tests, however, repeated loading can lead to substantial self-heating of the concrete. The resulting temperature increase reduces the compressive strength and thereby increases the effective maximum stress level when the applied stress levels are kept constant. At low minimum stress levels, the corresponding increase in the effective minimum stress is comparatively small, resulting in an increased effective stress range and, consequently, a reduced fatigue life. Here, $S_{\min}$ and $S_{\max}$ denote the minimum and maximum compressive stress level, respectively, normalized by the concrete compressive strength. A comprehensive discussion of specimen heating during concrete fatigue tests is provided in [45,47].

Other factors, such as load sequence effects [48] and the interaction between reinforcement and concrete under fatigue loading [49], are beyond the scope of the present study and are therefore not considered further.

The reviewed literature indicates that the fatigue life of concrete is influenced by its composition. A better understanding of the relationship between concrete composition and fatigue life could provide a basis for assessing the adequacy of current safety factors and developing more economical and sustainable fatigue design approaches. Such an assessment requires a sufficiently large database covering a broad range of concrete compositions and stress levels under comparable test conditions. To date, neither such a database nor data-driven methods for predicting concrete fatigue life based on concrete composition are available in the literature.

To address these research gaps, a database of fatigue tests on 18 different high-strength concrete compositions, conducted under comparable experimental conditions, was first compiled and systematically analyzed in this work. The database was then used to identify the key concrete composition parameters influencing the number of cycles to failure and to quantify their relationships with fatigue life by using correlation analyses. Next, the potential of machine learning methods for predicting the number of cycles to failure based on concrete composition was investigated. Such an approach could enable the fatigue performance of a concrete composition to be assessed prior fatigue testing and could support the targeted optimization of concrete compositions for improved fatigue performance. Machine learning has already been successfully applied to predict concrete compressive strength based on mixture composition [50–52]. More recently, physics-based machine learning approaches have been developed to predict concrete fatigue life under non-uniform cyclic loading [53] and to accelerate fatigue damage evolution and lifetime prediction using physics-constrained neural networks [54]. Bayesian updating has also been used to develop probabilistic S–N relationships for reinforced-concrete beams exposed to chloride attack [55], while multiscale physical neural networks have been proposed for multiaxial fatigue-life prediction [56]. Unlike these approaches, the present study compares different data-driven machine learning models trained on experimental fatigue tests of high-strength concrete to quantify the additional predictive value of concrete composition alongside stress levels and concrete age.

2. Methodology

The methodology adopted in this study, with a particular focus on the influence of concrete composition, can be divided into five main stages, ranging from experimental testing to the prediction of the number of cycles to failure using a machine learning approach, as illustrated in Fig. 1. The five stages are described in detail in the following paragraphs, beginning with the experimental testing and followed by the estimation of the number of cycles to failure, data normalization, correlation analysis, and the machine learning approach.

Experimental testing: A total of 241 cylindrical concrete specimens were subjected to cyclic compressive loading. The specimens were tested at different stress levels. The database comprised 18 different concrete compositions, all classified as high-strength concrete. At least three fatigue tests were conducted for each composition and compressive stress level. Normal-strength and ultra-high-strength concretes were deliberately excluded from the present analysis to limit the scope of the investigation and to ensure a consistent strength range within the database. Detailed information on the specimen preparation, fatigue testing procedure, loading conditions, and measurement equipment is provided in Chapter 3.

Estimation of fatigue life: To limit the duration of the fatigue tests, predefined run-out levels were applied. Consequently, the actual number of cycles to failure was not experimentally determined for some specimens. For these tests, the number of cycles to failure was estimated based on the strain development at the maximum stress level and the Sparks–Menzies ratio [57]. This approach was adopted based on the assumption that the strain development provides a reliable basis for estimating the number of cycles to failure for the concretes investigated in this study. Its applicability to other concrete types has previously been demonstrated [58,59]. Following the estimation of fatigue life for the terminated tests, an outlier analysis was performed separately for each concrete composition and compressive stress level using the median absolute deviation. Identified outliers were excluded from the subsequent analyses to minimize the influence of anomalous test results on the statistical and machine learning analyses (Section 3.2).

Data normalization: As the fatigue tests were conducted at different compressive stress levels, the experimentally determined numbers of cycles to failure cannot be directly compared in a correlation analysis to assess the influence of concrete composition. Without normalization, separate correlation analyses would be required for each stress level, substantially reducing the number of data points available for each analysis. Therefore, the fatigue lives, including the estimated values, were normalized with respect to the S–N relationship specified in Model Code 2020 [9]. Among the investigated design provisions, the Model Code 2020 S–N curves showed the best agreement with the experimentally determined fatigue lives and were therefore selected as the reference for normalization (Section 3.3).

Correlation analysis: Correlation analyses were performed using the normalized number of cycles to failure to investigate its relationships with the variables included in the database. The investigated variables were divided into two groups: test-related variables and concrete composition variables. Test-related variables describe the experimental conditions, whereas composition-related variables describe the constituents and properties of the concrete compositions. The correlation analysis was used to assess both the strength and direction of the relationships with fatigue life. This allowed variables to be identified for which higher or lower values were associated with an increase or decrease in the number of cycles to failure. Spearman's rank correlation coefficient [60] was used because nonlinear and monotonic relationships between the investigated variables and fatigue life were expected (Chapter 4).

Machine learning based fatigue life prediction: Six machine learning approaches were implemented to predict the logarithm of the number of cycles to failure (decision trees, linear regression models, Gaussian process regression (GPR), support vector machine regression (SVR), artificial neural networks (ANN), and an LSBoost-based ensemble of regression trees). The machine learning models were trained using the concrete composition features, concrete age and the applied compressive stress level as input features, based on data from 16 of the 18 concrete compositions. The logarithm of the experimentally determined or estimated number of cycles to failure was used as the target variable. The available data were randomly divided into training and test datasets using a ratio of 80:20. The random partitioning was repeated for multiple model runs, resulting in different training and test datasets for each run. This approach was used to reduce the dependence of the model evaluation on a single random data split. Prior to model training, the input features were normalized. Hyperparameter optimization was performed to determine suitable model configurations for the individual machine learning approaches. The predictive performance of the models was evaluated using the coefficient of determination R^2, mean squared error (MSE), and mean absolute error (MAE). In addition to the predictive performance, feature importance was evaluated to identify the features that contributed most strongly to the model predictions. For model validation, the two concrete compositions that had been entirely excluded from model development were used to predict their respective fatigue lives. The predicted fatigue lives were then compared with the experimentally determined fatigue lives to assess the predictive

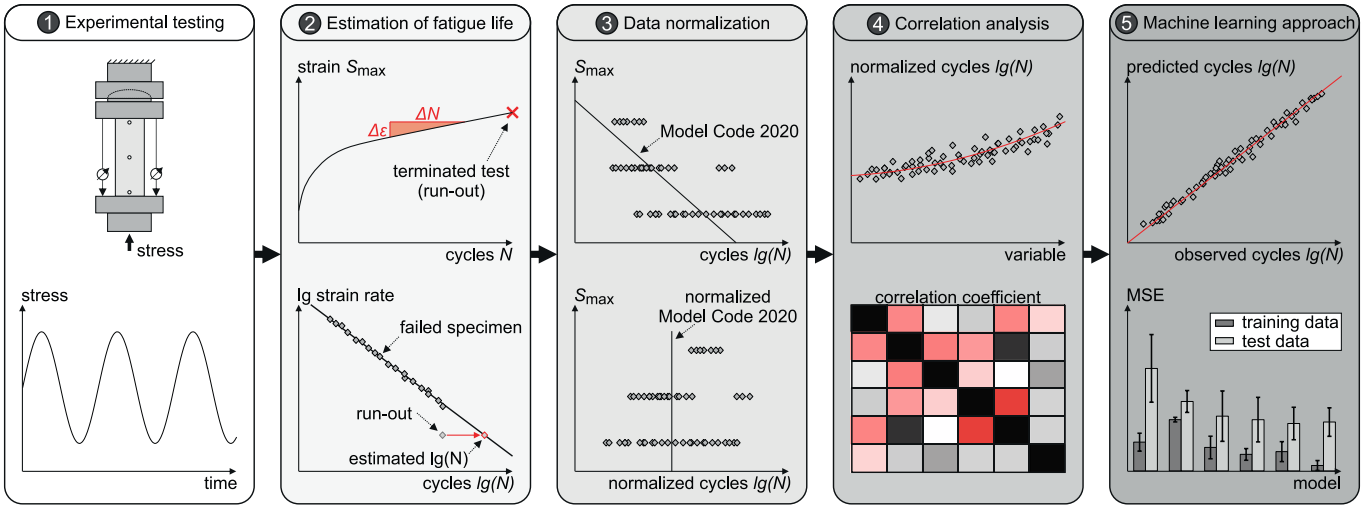

Fig. 1. Methodological workflow from experimental testing to fatigue life prediction using correlation analysis and machine learning (graphic: Sören Voß).

performance of the models for previously unseen concrete compositions within the parameter range represented in the training dataset (Chapter 5).

As a supplementary analysis, the temperature development of the concrete specimens during cyclic loading was evaluated. The temperature was measured at the surface of the specimen at approximately half of its height. The analysis was performed to assess the extent of specimen heating caused by cyclic loading and its potential influence on the measured fatigue life. The results of the temperature analysis and its relationship with the number of cycles to failure are provided in the Appendix.

3. Database and data preprocessing

3.1. Experimental campaign

A database comprising 241 fatigue tests on concrete subjected to cyclic compressive loading was compiled from experimental investigations conducted at the Institute of Concrete Construction at Leibniz University Hannover and the Institute of Concrete Structures at TU Dresden between 2015 and 2025. The database includes tests on high-strength concrete using cylindrical specimens with a height-to-diameter ratio of 3 and dimensions of 300 mm × 100 mm. The tests were conducted at frequencies of 4 or 5 Hz and at different compressive stress levels. To minimize potential size effects associated with different specimen dimensions [61,62], only specimens with identical dimensions were included in the present analysis. A total of 217 specimens from 16 concrete compositions were used for the correlation and machine learning analyses, as detailed in Table 1. Two additional concrete compositions, comprising 24 specimens, were used exclusively for validation of the machine learning predictions. The compressive stress levels considered for these specimens are listed in Table 2. At least three fatigue tests were performed for each concrete composition and compressive stress level. The database comprises 18 concrete compositions that differed in the type and content of the raw materials used.

The fatigue tests were conducted under force control using servo-hydraulic testing machines (Fig. 2, left). During the tests, at least three laser distance sensors were used to measure circumferential changes in length, and temperature sensors were used to measure temperature changes of the specimen surface (Fig. 2, right). To determine the compressive stress levels, uniaxial short-term compressive strength tests were conducted on at least three specimens with the same dimensions from each batch, immediately before the fatigue tests. For test series extending over approximately four weeks, new reference compressive strengths were determined at later concrete ages to account for continued hydration and the associated increase in compressive strength. To limit test duration, predefined run-out levels were established for each compressive stress level. Once the specified run-out level was reached, the test was terminated and classified as a run-out. The predefined run-out level can be found in the Appendix (Table 6).

The data set is presented in Fig. 3. The experimentally determined number of cycles to failure were compared with *S-N* curves based on current regulations of Model Code 1990 [8], Model Code 2020 [9], and Eurocode 2 [10]. A distinction was made between failed and specimens reaching run-out level for the individual fatigue tests. Here, the compressive stress levels exhibit different fatigue sensitively. Numerous run-out specimens occur at $S_{min}/S_{max} = 0.05/0.60$ and 0.20/0.70. However, 40 out of 52 test specimens failed at the compressive stress level of $S_{min}/S_{max} = 0.05/0.70$. For individual concrete compositions and specimens, an early fatigue failure was observed, with some test results even falling below the S–N curve of Model Code 1990, which may be associated with unfavorable concrete compositions, constituent materials, or their respective contents.

Table 1
Number of concrete compositions tested at each compressive stress level used for correlation and machine learning analyses.

S_{min}/S_{max}	0.05/0.60	0.05/0.70	0.05/0.80	0.20/0.70	0.20/0.80	0.40/0.80
Number of concrete compositions tested	16	16	2	16	2	16

Table 2
Number of concrete compositions tested at each compressive stress level used exclusively for validation.

S_{min}/S_{max}	0.05/0.60	0.05/0.65	0.05/0.75	0.20/0.75	0.40/0.80
Number of concrete compositions tested	1	1	2	2	2

Fig. 4 provides a more detailed analysis of the concrete compositions. It shows the normalized proportion of run-out specimens and fatigue tests that reached the level defined in Model Code 2020, categorized by concrete composition. For example, 0.83 of concrete composition 1 specimens exceeded the number of cycles to failure according to the Model Code 2020 [9], and 0.44 of concrete composition 1 specimens reached run-out level. On average, approximately 0.66 of fatigue tests reached the level defined in Model Code 2020 [9] (light gray horizontal line in Fig. 4), which highlights the fundamental suitability of the *S-N* curves for high-strength concretes. All specimens of five concrete compositions reached at least the Model Code 2020 level. For three of these compositions (10, 15, and 16), all tests were stopped in accordance with the termination criterion, and all test specimens were classified as run-out. However, it also became apparent that for some concrete compositions—no. 13 and 18, for example—many test specimens failed before reaching the level defined in Model Code 2020 [9].

A comparison of the determined mean values with the *S-N* curves according to Model Code 1990 [8] (Fig. 3) revealed that, with the exception of the compressive stress level $S_{min}/S_{max} = 0.05/0.60$, the number of cycles to failure for all concrete compositions examined lay above the Model Code 1990 curves. This indicates that Model Code 1990 tends to underestimate the actual, experimentally determined number of cycles to failure for almost all considered compressive stress levels.

The observed differences in fatigue life may be related to differences in concrete composition. The fatigue tests were conducted under comparable experimental conditions, supporting this assumption. To investigate the potential causes of the observed differences, all influencing factors systematically recorded in the database were considered. These factors include concrete composition, specimen quality and preparation, test procedure parameters, and fatigue behavior characterized by strain, stiffness, and temperature development.

3.2. Estimation of number of cycles to failure for specimens reaching run-out

The numbers of cycles to failure are of central importance for a targeted analysis of potential factors influencing fatigue life. For this reason, the numbers of cycles to failure for the run-out specimens were predicted, [63,64], based on strain development during fatigue tests of concrete under cyclic compressive loading e.g., [65–67] (Fig. 5, left). The three phases are associated with progressive material degradation. In phase I, intensive microcrack formation and stress redistribution occur within the material. Once these processes stabilize, crack formation intensifies continuously in phase II. Phase III is characterized by the development of macrocracks, which ultimately lead to specimen failure [65,66]. The stiffness over the test duration exhibits a similar behavior [68].

Based on this well-known behavior, the numbers of cycles to failure for specimens that reached run-out were estimated using the strain rate during phase II, following the approach described in [58], which

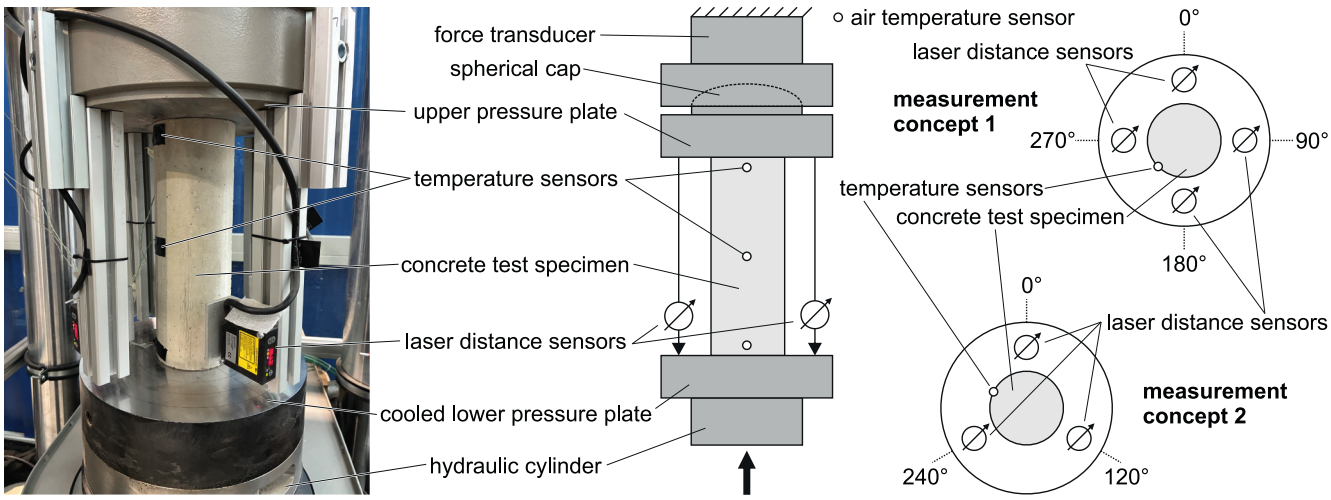

Fig. 2. Experimental setup and measurement concept, as well as the two configurations of the laser distance sensors used to measure longitudinal strains (photo/graphic: Sören Voß).

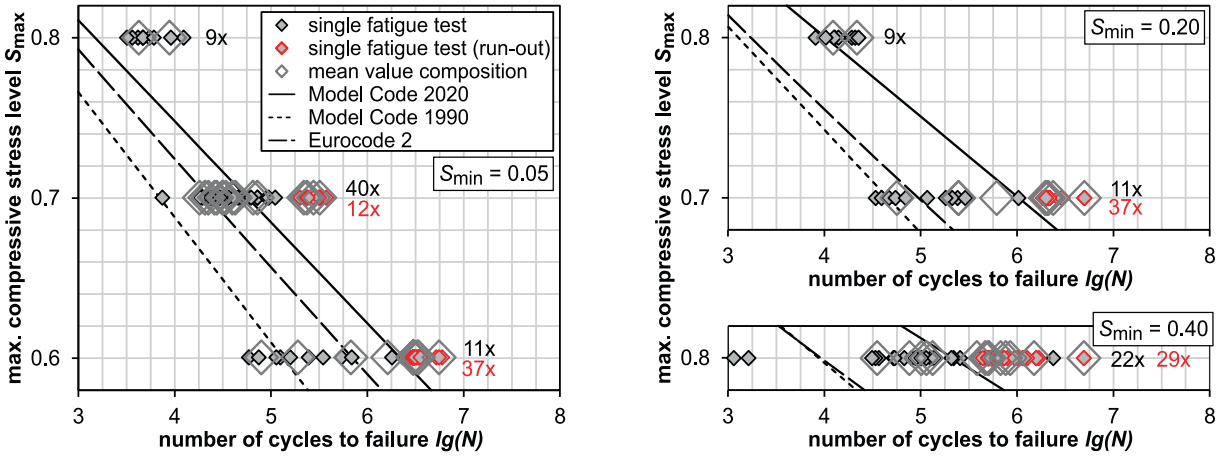

Fig. 3. Summary of results from the fatigue tests conducted, including the number of failed specimens and run-out specimens for each compressive stress level (graphic: Sören Voß).

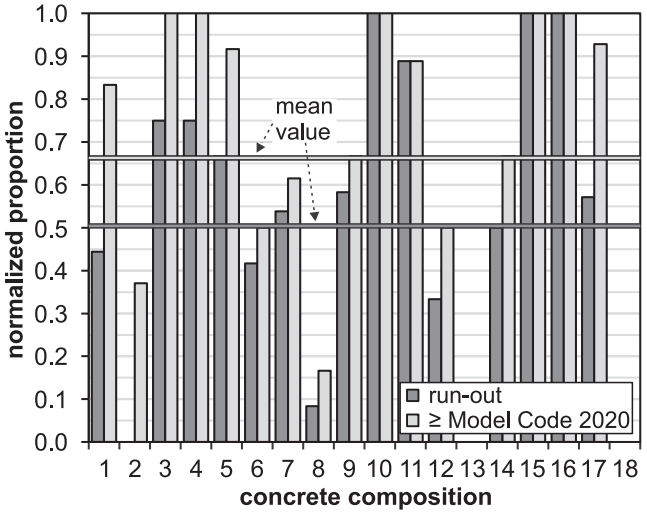

Fig. 4. Normalized proportion of fatigue tests per concrete composition in which the number of cycles to failure was underestimated by the *S-N* curves according to Model Code 2020 (≥ Model Code 2020; light gray) and those classified as run-out (dark gray; graphic: Sören Voß).

demonstrated the robustness of strain-based fatigue-life estimation. The strain rate in phase II is largely independent of the run-out level and can therefore be reliably determined from terminated fatigue tests, provided that phase II has been reached. Phase II is characterized by an approximately linear increase in strain with the number of cycles. For normal-strength concrete, phase transitions are often assumed to occur at 20% and 80% of number of cycles to failure; for concretes with higher strengths, shorter phases I and III were observed [69–72]. For run-out specimens, the thresholds must be adjusted to ensure the strain rate was determined in the linear phase II.

For each test specimen, the strain development during the fatigue test was evaluated based on the mean deformation measured by the laser sensors. The strain rate during phase II at maximum compressive loading was determined as illustrated in Fig. 5 (right) using a double-logarithmic representation. The specimens were divided into two groups according to whether they reached failure or were terminated at the predefined run-out level. For the specimens that reached failure, regression relationships between the logarithm of the strain rate and the logarithm of the number of cycles to failure were established separately for each concrete composition to account for potential composition-dependent differences in strain development. These regression relationships were subsequently used to estimate the number of cycles to failure for specimens terminated at the run-out level based on their respective strain

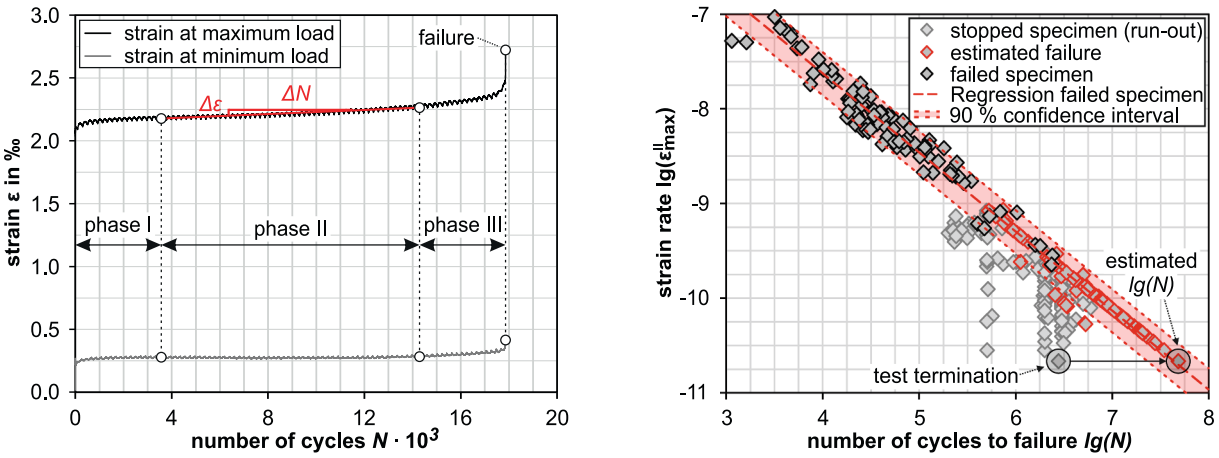

Fig. 5. Exemplary strain development under single-stage fatigue loading at minimum and maximum load levels (left), and Sparks-Menzies relation (right; graphic: Sören Voß).

rates. This procedure corresponds to a shift of the respective data points toward higher numbers of cycles to failure [58], as illustrated by a selected test specimen in Fig. 5 (right). If no failed specimen was available for a particular concrete composition, the regression relationship established using the combined dataset of all concrete compositions was used for the estimation. If the predicted number of cycles to failure was lower than the number of cycles already reached at test termination, the experimentally reached number of cycles was retained as the estimated fatigue life. This situation may occur when a test is terminated shortly before failure or due to variations in the determination of the strain rate. The 90% confidence interval for the failed specimens shown in Fig. 5 (right) indicates that deviations in the estimated strain rate can occur without necessarily representing erroneous measurements.

The predicted number of cycles to failure revealed that some test specimens were close to failure when terminating the fatigue test, while others stopped well before potential failure. Therefore, the selected run-out level significantly underestimates the actual number of cycles to failure for some test specimens. Taking the predicted number of cycles to failure into account, the mean values for the individual concrete composition were determined (Fig. 6). This further highlights the significant differences in fatigue life among the examined concrete compositions.

Next, the dataset was checked for outliers separately for each concrete composition and compressive stress level. Outlier classification was based on the median absolute deviation, using a threshold value of 3. Specimens classified as outliers were completely excluded from all subsequent analyses. In total, 22 of the initial 217 fatigue tests were excluded, leaving 195 tests for the correlation and machine-learning analyses. Of the remaining 195 tests, 94 fatigue lives were observed experimentally, while 101 were estimated (Appendix Table 5).

3.3. Normalization of number of cycles to failure

To enable a comprehensive analysis of the entire dataset, the logarithm of the number of cycles to failure was normalized with respect to the logarithmic S–N curve specified in Model Code 2020 (Fig. 7). The normalization was performed by dividing the experimentally determined logarithmic fatigue life by the logarithmic fatigue life according to Model Code 2020 $(lg(N_{exp})/lg(N_{MC2020}))$. A normalized logarithm of the number of cycles to failure of 1 indicates that the experimentally determined fatigue life corresponds to the fatigue life predicted by Model Code 2020 at the respective compressive stress level. Model Code 2020 was selected after comparing its *S–N* curve with those specified in Eurocode 2 and Model Code 1990. It showed the most consistent overall agreement with the experimental fatigue lives across the investigated compressive stress levels, whereas Model Code 1990 tended to underestimate the observed fatigue lives and Eurocode 2 showed less consistent agreement. Model Code 2020 was therefore considered the most suitable reference for the present dataset. This normalization provides a common reference for comparing the fatigue lives of specimens tested at different stress levels and enables the subsequent correlation analysis.

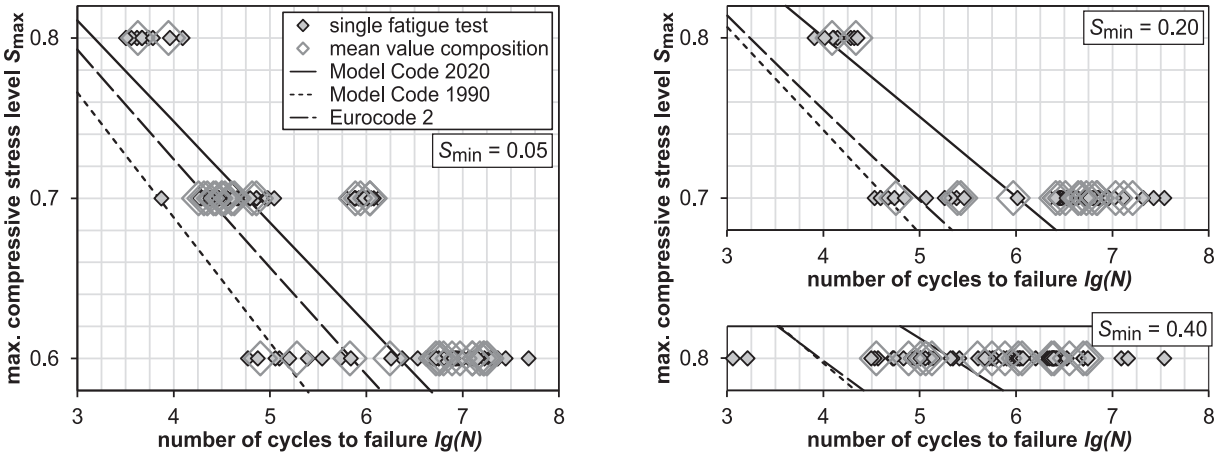

Fig. 6. Summary of results from fatigue tests conducted, after estimating the number of cycles to failure of specimens that reached the run-out level (graphic: Sören Voß).

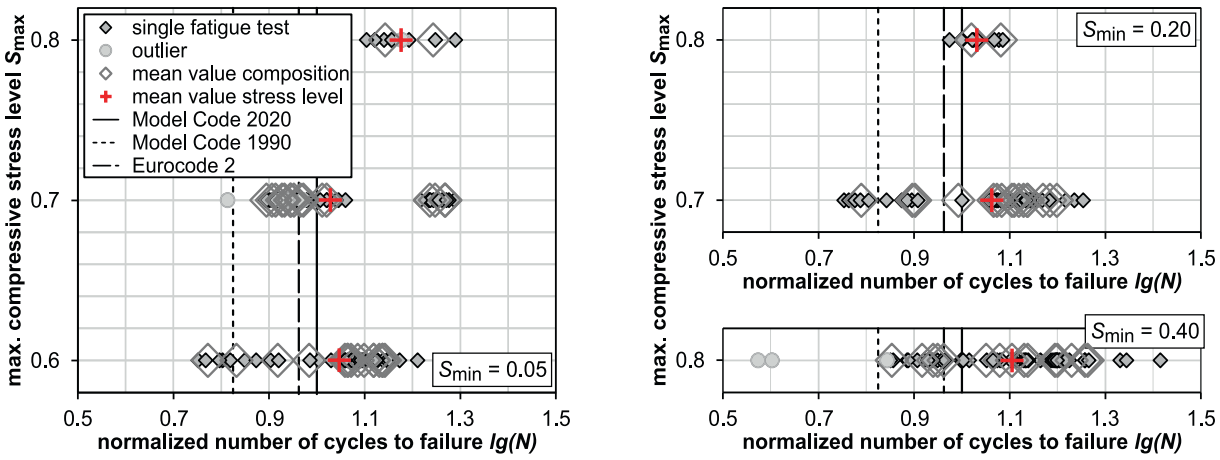

Fig. 7. Summary of results from the conducted fatigue tests after normalizing the logarithmic numbers of cycles to failure based on the logarithmic *S-N* curve according to Model Code 2020 (graphic: Sören Voß).

An analysis of the mean normalized numbers of cycles to failure at each compressive stress level shows that, among the compressive stress levels with a sufficient number of test results, the lowest number of cycles to failure occurred at $S_{min}/S_{max} = 0.05/0.70$ and the highest at $S_{min}/S_{max} = 0.40/0.80$. The compressive stress levels $S_{min}/S_{max} = 0.05/0.80$ and 0.20/0.80 were excluded from this comparison because only a very limited number of test results were available. The observed trend is assumed to be related to the temperature increase during cyclic loading, which is discussed in more detail in the Appendix.

4. Correlation analysis and feature selection

4.1. Test condition analyses

The normalized numbers of cycles to failure determined in Section 3.3 were used for the correlation analyses. They are plotted in Fig. 8 and Fig. 9 against various potential influencing variables. The normalization of the number of cycles to failure enables the entire database to be analyzed jointly while accounting for differences resulting from the applied compressive stress levels. Without normalization, separate correlation analyses would be required for each compressive stress level, resulting in smaller datasets and potentially different or inconsistent relationships. All potential influencing variables that could be derived from the available database were considered. In addition to the individual fatigue tests and identified outliers, Fig. 8 and Fig. 9 present the mean values for each concrete composition, a second-order polynomial fitted to the mean values, and the corresponding 90% confidence interval based on the assumption of a normal distribution. Where an insufficient number of data points was available to reliably fit a second-order polynomial, a linear regression was used instead.

The mean compressive strength of the additional test specimens (Fig. 8**a**) and the bulk density (Fig. 8**b**) are within the expected range. Furthermore, no discernible correlations are evident. The weak correlation between compressive strength and normalized fatigue life is consistent with recent findings showing that high-strength and ultra-high-strength concretes do not exhibit an increased fatigue sensitivity compared with normal-strength concretes [12]. Since the present dataset comprises exclusively high-strength concretes with relatively

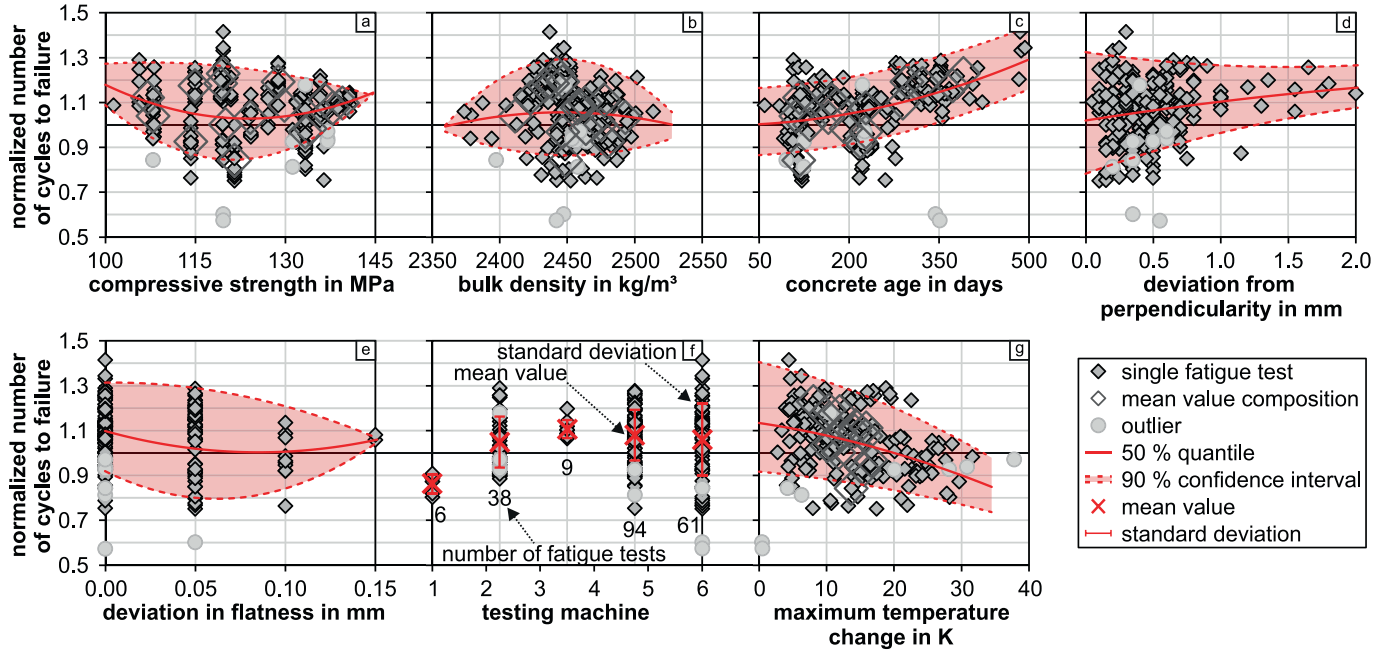

Fig. 8. Correlation diagrams of potential influencing variables identified from the experimental results (graphic: Sören Voß).

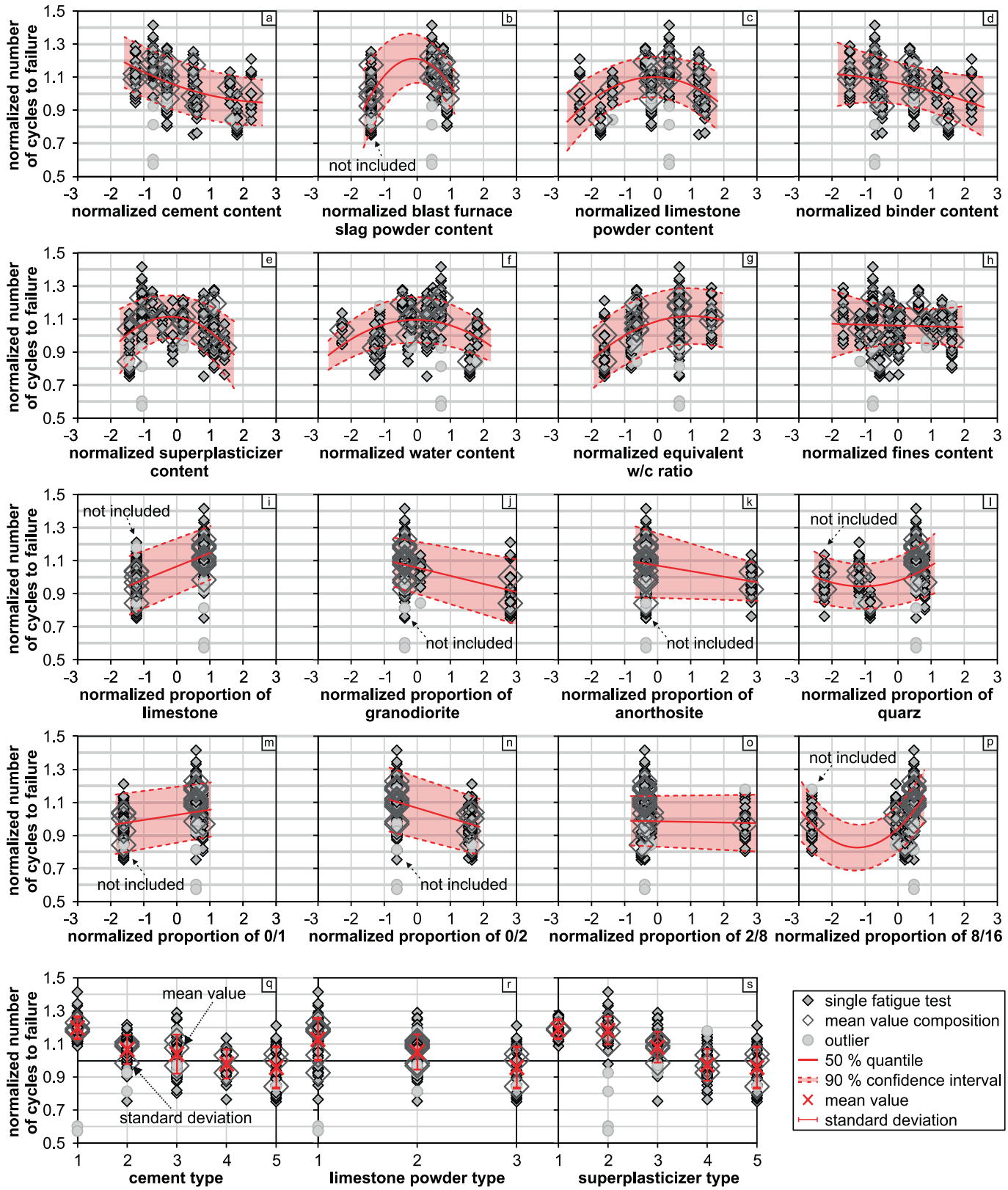

Fig. 9. Correlation diagrams of potential influencing variables dependent on concrete composition; data points annotated as "not included" represent concrete compositions in which the respective variable is absent (graphic: Sören Voß).

small differences in compressive strength, an independent influence of compressive strength on fatigue life is expected to be limited and cannot be reliably identified. Continued strength development due to post-curing is unlikely to explain the observed increase in fatigue life with concrete age, as the compressive strength used to determine the compressive stress level was measured immediately before fatigue testing (Fig. 8**c**). A possible explanation is that ongoing hydration and the associated increase in the strength of the hardened cement paste

reduce the stiffness contrast between the cement paste and aggregate, resulting in a more homogeneous microstructure. This may reduce local stress concentrations and consequently increase fatigue life, as discussed in Chapter 1. However, as concrete age and compressive strength development are interrelated, their individual contributions to fatigue life within a given concrete batch cannot readily be distinguished.

To eliminate the possibility that the number of cycles to failure depends on specimen preparation (see [43]), the perpendicularity and flatness of the load application areas were examined in detail according to DIN EN 12390-1 [73]. Prior to testing, these areas of the test specimens were ground to ensure sufficient perpendicularity to the lateral surface. Excessive deviations could result in eccentric load distribution, which can lead to premature failure. However, no negative influence of perpendicularity deviation on the normalized number of cycles to failure was observed for the test specimens examined in the presented study (Fig. 8**d**). Rather, an increase in the normalized number of cycles to failure was observed. However, comparatively few tests with higher perpendicularity deviations are contrasted with a large number of tests with small deviations. These few tests ultimately influence the regression curve significantly. This increase is implausible and illustrates the weakness of this form of analysis. In addition to verifying perpendicularity, the load application area must be sufficiently flat to enable uniform force transmission from the testing machine's pressure plates to the test specimen. This prevents local stress concentrations. The deviation from ideal flatness was manually measured for all test specimens and evaluated with the normalized number of cycles to failure. As the flatness deviation increases, the results show a slight decrease in the normalized number of cycles to failure. These results fall within the normal range of variation (Fig. 8**e**).

Three different hydraulic testing machines were used primarily for the fatigue tests (Fig. 8**f**). At least two different testing machines were used to conduct tests on each concrete composition. To evaluate the potential influence of the testing machine, the mean and standard deviation of the normalized numbers of cycles to failure were used. Results from machines 2, 4, and 6 show that the mean and standard deviations are approximately the same, indicating no discernible influence of the machine used. However, the maximum temperature change (Fig. 8**g**), which was measured during the fatigue test, indicates a clear reduction in the normalized number of cycles to failure as the temperature change increases (see also Appendix). Based on the database, it can be assumed that the number of cycles to failure was independent of specimen preparation or the testing machine used.

4.2. Concrete composition analysis

The following analysis focuses on the influence of concrete composition, as shown in Fig. 9. As a first step, the composition variables were normalized to obtain a common scale with a mean of zero and a standard deviation of one. The diagrams can be divided into three groups. The first two rows (Fig. 9**a–h**) show different proportions of the concrete constituents. The third and fourth rows (Fig. 9**i–p**) present the types and quantities of aggregates, while the fifth row (Fig. 9**q–s**) shows the effects of different raw material types. The individual composition variables cannot be considered independently because changes in one constituent generally require corresponding adjustments to other constituents. For example, an increase in cement content is accompanied by changes in the contents of other components, such as limestone powder, blast furnace slag powder, water, and superplasticizer. Consequently, the decrease in normalized fatigue life observed with increasing cement content in Fig. 9**a** is also associated with decreasing limestone powder content (Fig. 9**c**) and increasing water content (Fig. 9**f**). Therefore, the observed decrease in normalized fatigue life cannot be uniquely attributed to a single composition variable. Instead, it may result from the individual or combined effects of cement, limestone powder, water, and other correlated composition variables.

The different raw material types shown in the fifth row (Fig. 9**q–s**) were assigned numerical labels for visualization only. These labels distinguish the individual material categories and do not represent quantitative material properties or physically meaningful distances. For cement, limestone powder, and superplasticizer type, neither a mean curve nor a confidence interval was calculated because these statistical representations are not meaningful for nominal categorical variables and could lead to misinterpretation. Instead, the influence of the individual raw material types was illustrated using their respective mean values and standard deviations.

Despite their interdependence, certain trends can be identified among the variables. However, these trends should be interpreted as statistical associations rather than independent effects of individual mixture components, as several composition-related parameters vary simultaneously. Consequently, the observed correlations do not imply that changing an individual component alone would necessarily improve or impair fatigue performance. As the cement content increases (Fig. 9**a**) and hence also the binder content rises (Fig. 9**d**), the normalized number of cycles to failure decreases. The results for the contents of blast furnace slag powder (Fig. 9**b**), limestone powder (Fig. 9**c**), superplasticizer (Fig. 9**e**), and water (Fig. 9**f**) are uniformly distributed across the variable range. No distinct trends or dependencies were noticeable. As the equivalent water-to-cement ratio increases (Fig. 9**g**), fatigue life improves, contradicting findings in the literature [16,27]. All components with a particle size of less than 0.125 mm are summarized in Fig. 9**h** as the fines content. There is no apparent effect on the normalized number of cycles to failure.

The proportions shown in Fig. 9**i–p** represent the ratio of the mass of the variable under consideration to the total mass of the aggregate used. An increase in the normalized number of cycles to failure was generally observed when limestone (Fig. 9**i**) or larger proportions of quartz (Fig. 9**l**) were added. Using granodiorite (Fig. 9**j**) or anorthosite (Fig. 9**k**) as aggregate leads to a decrease in the normalized number of cycles to failure. However, since only two concrete compositions with each aggregate were tested, a reliable assessment is not possible at this time. All concrete compositions used either a 0/1 aggregate (Fig. 9**m**) or a 0/2 aggregate (Fig. 9**n**) as the fine aggregate. A higher normalized number of cycles to failure is shown by concrete compositions with a 0/1 aggregate. For the 2/8 and 8/16 aggregates (Fig. 9**o and p**), comparable proportions were used, with one exception, so no clear correlation with the normalized number of cycles to failure was apparent. Furthermore, clear dependencies in the type of raw materials can be observed (Fig. 9**q–s**).

4.3. Correlation coefficients

The correlation coefficients for the potential influencing variables listed in Sections 4.1 and 4.2 are presented below. Potential influencing variables that were assigned manually, such as the testing machine used or the type of raw material, were excluded from this analysis. The Pearson correlation coefficient r quantifies the strength and direction of a linear relationship between two variables and is calculated as the covariance divided by the product of their standard deviations. Since monotonic nonlinear relationships are predominantly expected, the Spearmańs rank correlation coefficient ρ was used instead [60]. Unlike the Pearson coefficient, the Spearman coefficient evaluates monotonic associations based on the ranks of the observations and can therefore capture monotonic relationships that are nonlinear.

The correlation coefficient can range from $\rho = -1$ to $\rho = 1$; a value of $\rho = -1$ or $\rho = 1$ indicates a perfect negative or positive correlation, respectively, and a value of $\rho = 0$ indicates an absence of correlation. Positive coefficients ($\rho > 0$) mean that as one variable's value increases, so does the correlated variable's value. Negative coefficients ($\rho < 0$), on the other hand, indicate that one variable decreases as the correlated variable's value increases. The Spearman correlation coefficients in Fig. 10 were calculated using individual specimen-level observations rather than composition-level averages. This approach retains the

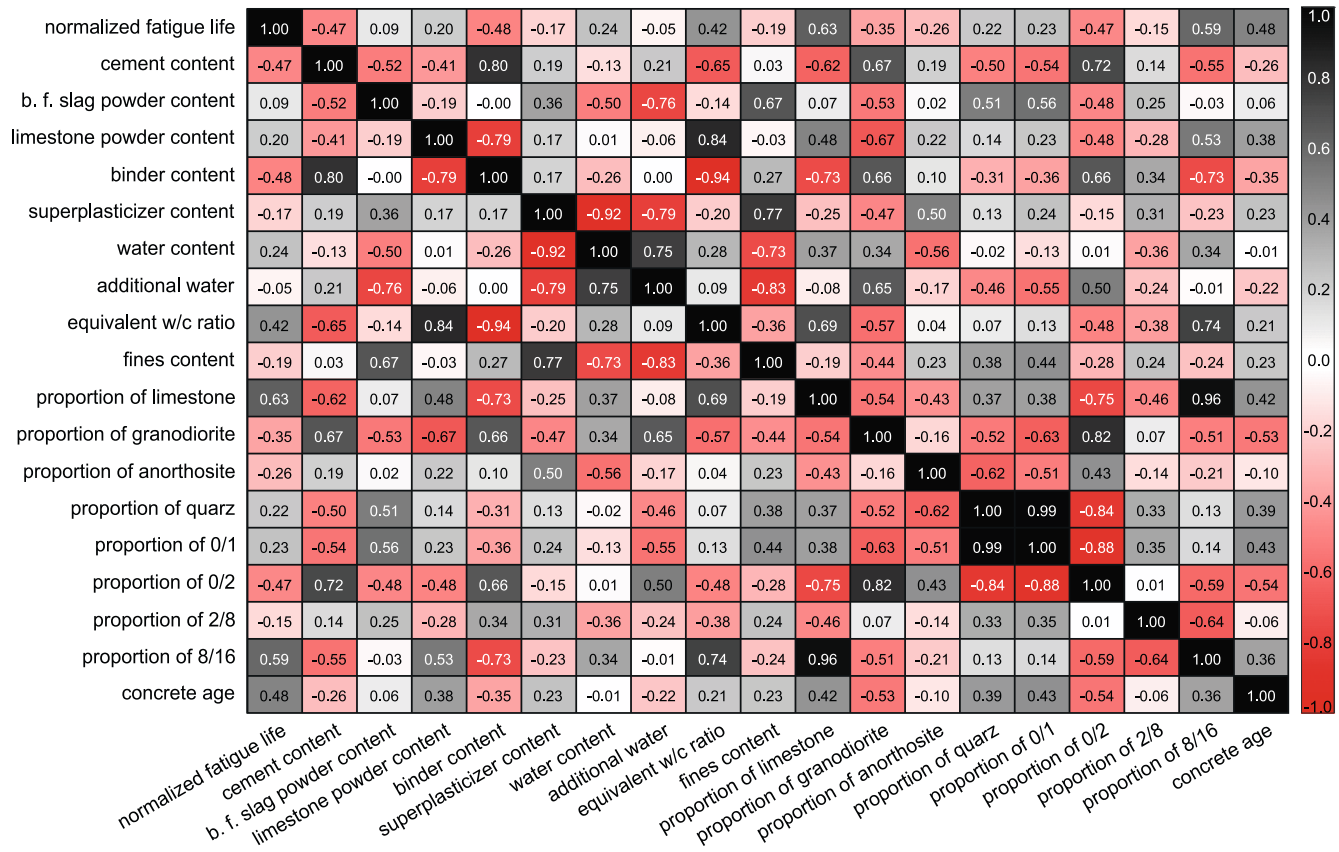

Fig. 10. Correlation matrix of various potential influencing variables based on Spearman (graphic: Sören Voß).

specimen-to-specimen variability in fatigue life.

As shown by the correlation analysis in Section 4.2, cement and total binder content, which are closely related variables, exhibit comparatively strong negative correlations with the normalized number of cycles to failure (Fig. 10). Thus, higher cement and binder contents are associated with lower normalized fatigue lives. The use of granodiorite and anorthosite as coarse aggregates is likewise associated with lower normalized numbers of cycles to failure, consistent with the findings presented in Section 4.2. The influence of the fine aggregate fractions 0/1 and 0/2 remains unclear, as their correlation coefficients cover both negative and positive values. This is consistent with the trends observed in Fig. 9**m,n**. The quartz content, limestone powder content, deviation from perpendicularity, blast furnace slag powder content, additional water, proportion of 2/8 aggregate, superplasticizer content, and fine aggregate content exhibit correlation coefficients close to zero, indicating no pronounced monotonic relationship with the normalized number of cycles to failure (Fig. 10). In contrast, the use of limestone as coarse aggregate, a higher proportion of 8/16 aggregate, and an increasing equivalent water-to-cement ratio are associated with higher normalized fatigue lives. Concrete age also exhibits a positive relationship with the normalized number of cycles to failure (Fig. 10).

The observed correlations between concrete composition variables and the number of cycles to failure should be interpreted with caution, as several composition-related variables are strongly interdependent (Fig. 10). For example, the quartz content shows a very strong positive correlation with the proportion of the 0/1 aggregate fraction ($\rho = 0.99$), while the equivalent water-to-cement ratio is strongly negatively correlated with the binder content ($\rho = -0.94$). Consequently, pronounced correlations between individual composition variables and the normalized number of cycles to failure may partly reflect their association with other composition variables rather than an independent effect of the respective variable. This limitation is particularly relevant for variables or material characteristics represented by only a small number of concrete compositions, such as granodiorite and anorthosite, for which only two compositions were investigated. The Spearman coefficients therefore indicate statistical associations within the investigated dataset and should be regarded as exploratory indications rather than robust or causal effects. Confirmation of the observed trends requires a larger dataset with systematically varied and independently controlled composition parameters.

5. Machine learning-based fatigue life prediction

The proposed machine-learning models use concrete composition, minimum and maximum compressive stress levels, and concrete age as input features (Fig. 11). his approach enables the prediction of fatigue life based on these input features and the underlying database. Within the parameter range represented in the database, the models may reduce the need for dedicated fatigue tests for each new combination of these input features. However, experimental data remain essential for model development and validation, and reliable predictions for substantially different concrete compositions cannot be assumed without further validation.

For example, the maximum temperature change was excluded as an input feature for the machine learning approach even though it significantly influences the number of cycles to failure in laboratory experiments (see Appendix). The maximum temperature change plays a central role in understanding the underlying fatigue failure mechanisms and improves the predictive quality of the machine learning approach. However, since the maximum temperature change is not known until after the fatigue test is finished, it is not considered in subsequent analyses. Consequently, specimens with identical concrete composition, stress level, and age receive identical input features and therefore the same predicted fatigue life. The inherent specimen-to-specimen scatter

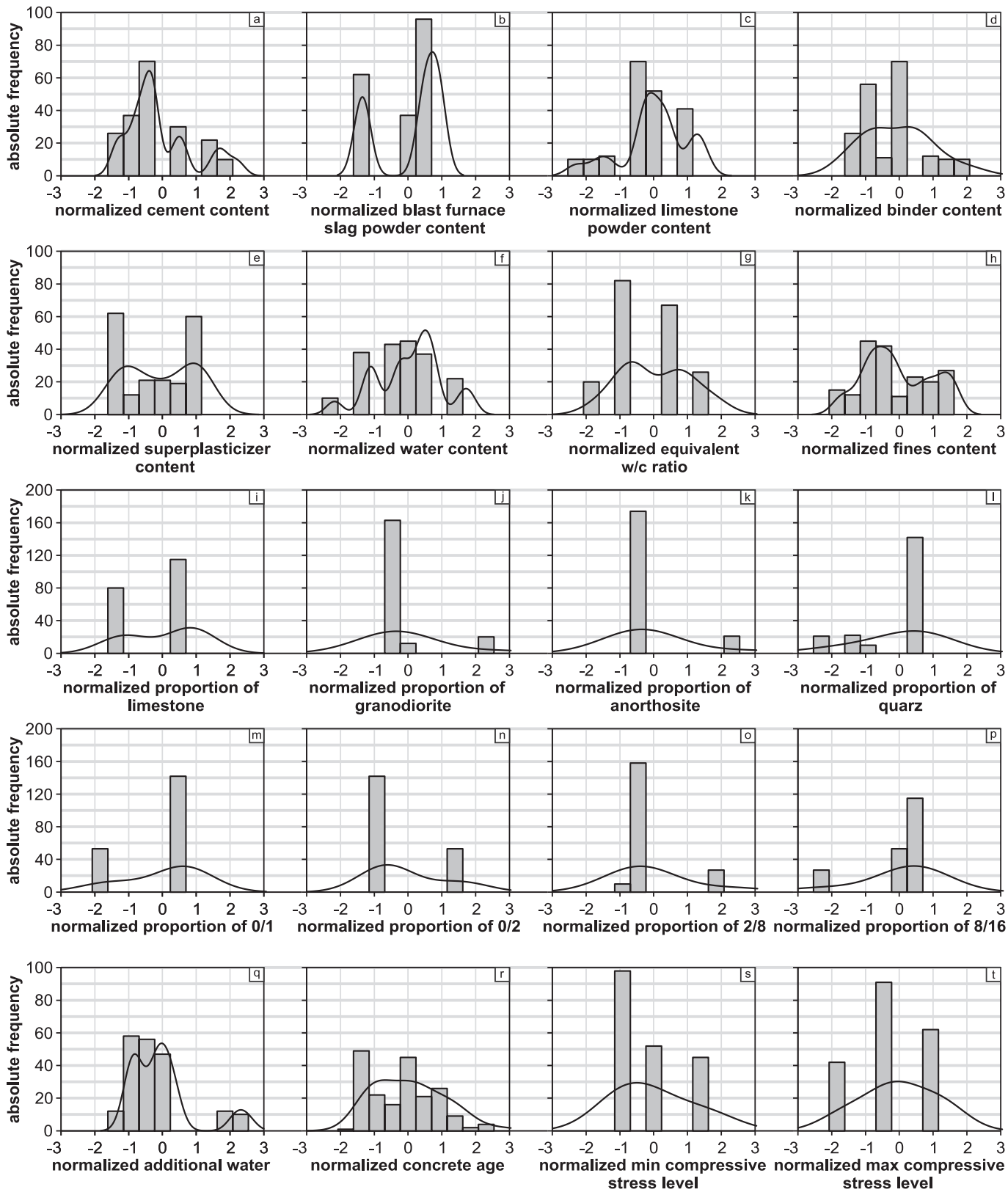

Fig. 11. Histograms and frequency distributions of the features (graphic: Sören Voß).

cannot therefore be captured by the present model. Including the temperature change could potentially address this limitation, as it may provide additional information on the individual damage evolution of the specimens.

On the other hand, concrete age was selected as an input feature. Although this parameter is only available within the context of the test procedure, it was nevertheless included in the machine learning approach. Since the time of construction—for example, of a wind energy turbine—and thus the start of cyclic loading on the concrete can be chosen within certain limitations, the concrete's fatigue life can be

influenced based on its time dependence without requiring additional measures. Therefore, in the fatigue test, the concrete's age can be equated with the time of construction to account for this influence. However, concrete age may also act as a proxy for differences between test campaigns, batches, or testing periods in the present database. Therefore, its predictive contribution cannot be attributed exclusively to age-related changes in the concrete, and the observed association should not be interpreted as evidence of an independent causal effect.

Unlike the correlation analyses, the machine learning models were trained using the actual number of cycles to failure. The applied compressive stress level was therefore included as an input feature to enable fatigue life prediction for a specific loading condition. This suggests that the models may also be capable of predicting the number of cycles to failure for compressive stress levels that differ from those directly represented in the database, provided that they remain within the range covered by the training data. The actual compressive strength was excluded as an input feature because its determination requires destructive testing. However, concrete age may indirectly capture some strength-related effects, such as a potential reduction in the stiffness contrast between the aggregate and cement paste due to continued strength development. In this way, the potentially beneficial effect of continued strength development on fatigue life may still be captured by the model.

The features shown in Fig. 11 were taken into account, as well as the types of cement, superplasticizer, and limestone powder. For each train-test split, all considered features were standardized to have a mean of $\sigma = 0.0$ and a standard deviation of $\mu = 1.0$. The means and standard deviations were calculated using the training data only and then applied unchanged to the corresponding test data. This ensured a consistent scale across the features while preventing information leakage from the test data during preprocessing. The input features are visualized using histograms and described in more detail using the kernel density estimate (KDE) [74]. The normalized input features for each concrete composition are listed in Table 7 in the Appendix.

The database was randomly divided into 80% training data and 20% test data for model development and evaluation. The machine learning models were implemented using MATLAB R2022a. Six approaches were considered to assess their suitability for predicting the number of cycles to failure: decision trees, linear regression models, Gaussian process regression (GPR), support vector machine regression (SVR), artificial neural networks (ANN), and an LSBoost-based ensemble of regression trees [75,76]. These approaches were selected to represent different model classes and to cover both linear and nonlinear relationships between the input features and fatigue life. For models with tunable hyperparameters, Bayesian optimization was employed to identify suitable hyperparameter configurations that improve predictive performance [77]. Further details on the models used can be found in Table 3.

Each model was trained 30 times using randomly training and test datasets. For each of the 30 training runs, the hyperparameter optimization was performed exclusively within the training data using five-fold cross-validation and Bayesian optimization. The optimized model was

Table 3
Machine-learning models and training settings.

Model	MATLAB function	Model architecture	Hyperparameter optimized	Optimization method	Validation
Regression tree	fitrtree	Single regression decision tree	-	No optimization	80/20 train-test split
Linear regression	fitrlinear	Regularized linear regression (least-squares learner)	Lambda	Bayesian optimization; expected-improvement-plus	5-fold CV; MSE
Gaussian process regression (GPR)	fitrgp	Gaussian process regression with a kernel-based covariance function	Sigma	Bayesian optimization; expected-improvement-plus	5-fold CV; MSE
Support vector regression (SVR)	fitrsvm	Support vector regression with a Gaussian (RBF) kernel	Box constraint; Kernel scale; Epsilon	Bayesian optimization; expected-improvement-plus	5-fold CV; MSE
Artificial neural network (ANN)	fitrnet	Feed-forward multilayer perceptron (MLP) with 1–3 hidden layers; optimized layer sizes and activation functions	Number of hidden layers; Layer 1 size; Layer 2 size; Layer 3 size; Activations; Lambda	Bayesian optimization; expected-improvement-plus	5-fold CV; MSE
LSBoost-based ensemble of regression trees	fitrensemble	Ensemble of regression trees using LSBoost	Method; Num learning cycles; Learn rate; Min leaf size	Bayesian optimization; expected-improvement-plus	5-fold CV; MSE

Table 4
Distribution of hyperparameters selected during the 30 independent optimization runs.

Model	Hyperparameter	Summary of hyperparameters across 30 training runs
Tree	-	-
Linear	Lambda	Median = $1.62 \bullet 10^{-5}$; Min = $6.48 \bullet 10^{-8}$; Max = $9.55 \bullet 10^{-3}$
	Learner	30 • Least squares
GPR	Sigma	Median = 0.379; Min = 0.212; Max = 0.860
SVR	Box constraint	Median = 671.43; Min = 1.47; Max = 975.36
	Kernel scale	Median = 12.57; Min = 0.43; Max = 23.85
	Epsilon	Median = $6.97 \bullet 10^{-3}$; Min = $1.70 \bullet 10^{-3}$; Max = 0.22
ANN	Number of hidden layers	Median = 2; Min = 1; Max = 3
	Layer 1 size	Median = 24; Min = 1; Max = 299; 30/30 runs
	Layer 2 size	Median = 23; Min = 2; Max = 297; 23/30 runs
	Layer 3 size	Median = 63; Min = 2; Max = 298; 14/30 runs
	Activations	15 • sigmoid; 8 • tanh; 6 • ReLU and 1 • none
	Lambda	Median = $3.83 \bullet 10^{-3}$; Min = $1.26 \bullet 10^{-6}$; Max = $2.71 \bullet 10^{-2}$
Ensemble	Method	30 • LSBoost
	Num learning cycles	Median = 201.5; Min = 11.0; Max = 499.0
	Learn rate	Median = 0.217; Min = 0.014; Max = 0.941
	Min leaf size	Median = 3; Min = 1; Max = 22

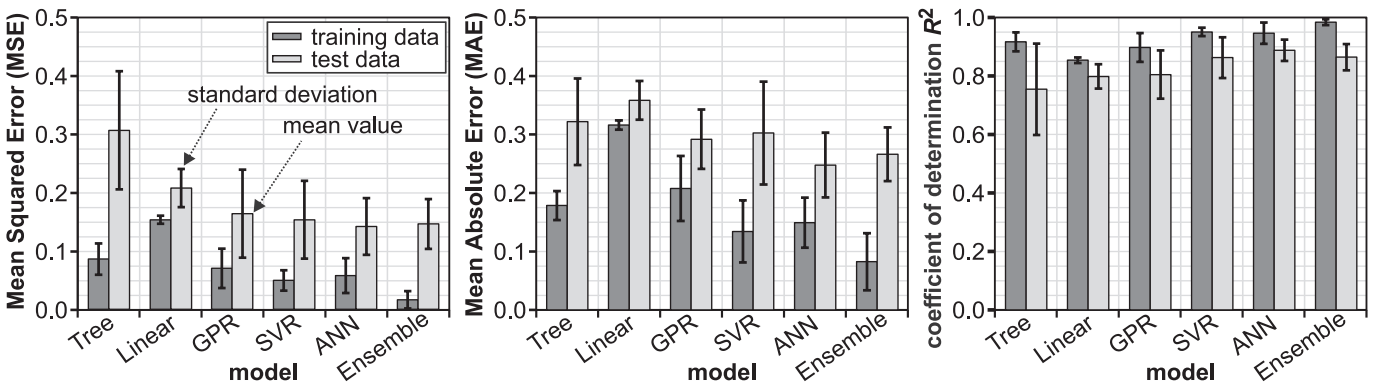

Fig. 12. Comparison of the mean squared errors (MSE), the mean absolute errors (MAE), and the coefficient of determination (R^2) obtained from 30 independent training runs (graphic: Sören Voß).

subsequently evaluated on the corresponding independent test set. A new random train-test split was generated for each training run. The hyperparameters considered from 30 training runs can be found in Table 4.

The mean squared error (MSE), mean absolute error (MAE), and coefficient of determination (R^2) were calculated for both the training and test datasets. The mean values and standard deviations obtained from the 30 training runs were used to assess the predictive performance and robustness of the individual models. Fig. 12 summarizes the resulting MSE, MAE and R^2 values as a function of the modeling approach. The ensemble-based model achieved the lowest MSE and MAE for the training data. For the test data, the artificial neural networks and ensemble-based models showed similarly low MSE and MAE values with comparatively low standard deviations. Based on their predictive performance and robustness, the ANN and ensemble-based models were selected for further analysis. The comparatively poor performance of the linear regression model suggests that linear relationships alone are insufficient to adequately describe the relationship between the investigated features and fatigue life. This nonlinearity may reflect the nonlinear stress–fatigue-life relationship, progressive microcrack initiation and propagation under cyclic compression, and interactions among composition-related features.

Fig. 13 compares the observed and predicted numbers of cycles to failure for the training and test datasets. The mean squared error (MSE), coefficient of determination (R^2), and 90% confidence interval based on a normal distribution were determined for both models. For the training data, the ensemble-based model achieved an R^2 of 0.992, while the artificial neural networks achieved an R^2 of 0.961, indicating a close agreement between the observed and predicted values. The models also showed good predictive performance for the test data, with R^2 values of 0.941 for the ensemble-based model and 0.906 for the artificial neural networks. Compared with the training data, the test data showed a slightly greater scatter, with individual predictions exhibiting larger deviations from the line of perfect agreement. This is also reflected in the corresponding prediction errors shown in Fig. 13 (bottom), which represent the deviation of the observed fatigue life from the predicted fatigue life, calculated as the observed fatigue life minus the predicted fatigue life. Nevertheless, both models maintained a high level of predictive accuracy for the previously unseen test data, indicating good generalization performance.

Fig. 14 shows the relative importance of the individual input features for predicting the number of cycles to failure, assessed using the RReliefF algorithm with ten nearest neighbors ($k = 10$) [78]. This method evaluates the predictive relevance of individual features based on local

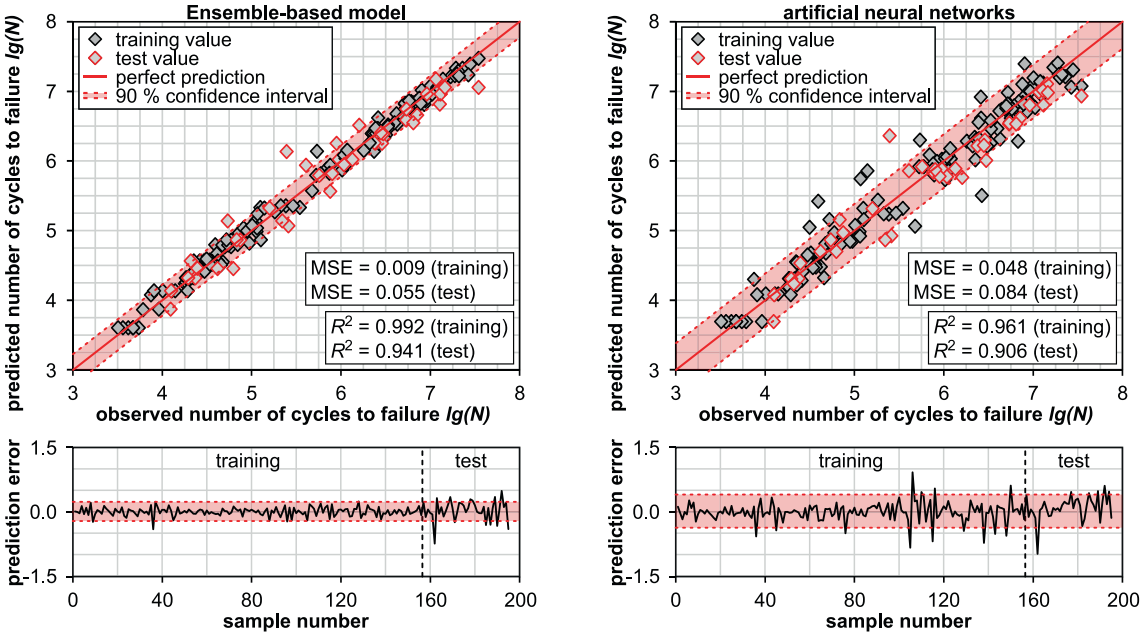

Fig. 13. Comparison of the predicted with the experimentally determined number of cycles to failure using the ensemble-based model (left) and artificial neural networks (right), as well as the prediction error for the training and test data (below; graphic: Sören Voß).

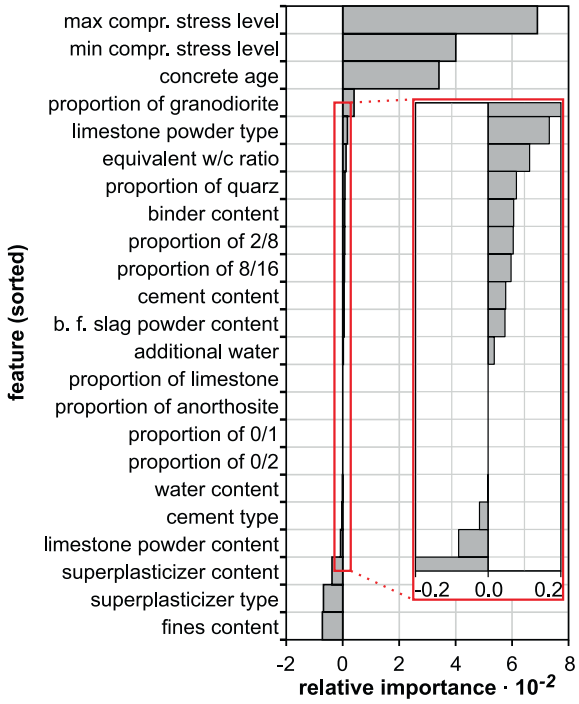

Fig. 14. Illustration of the importance of the selected influencing features for predicting the number of cycles to failure (graphic: Sören Voß).

relationships between neighboring observations. Higher positive scores indicate greater predictive relevance, whereas scores close to zero indicate limited relevance. Negative scores indicate that a feature is a poor predictor under the RReliefF criterion; they do not imply a physically adverse effect or a negative contribution to the predictions of the trained machine learning models. The maximum and minimum compressive stress levels were identified as the most influential features for predicting the number of cycles to failure. Concrete age also showed a substantial predictive relevance, consistent with the trend observed in the correlation analysis (Fig. 8**c**). In general, features exhibiting stronger correlations with fatigue life (Fig. 10) also tended to show greater importance in the machine learning model. In contrast, the amount and type of superplasticizer and the fine aggregate content showed comparatively low feature-importance scores. These low importance values do not necessarily imply that the corresponding parameters have no physical influence on fatigue life. Rather, their limited individual importance may reflect the dominant predictive contribution of compressive stress level and concrete age, as well as the interdependence among composition-related features, which may lead to overlapping predictive information. Furthermore, the limited number of investigated concrete compositions restricts the ability to identify the individual predictive contributions of mixture-proportion features.

To further investigate the contribution of composition-related features, particularly given the low individual feature-importance values observed for several of these features (Fig. 14), model performance was compared using progressively expanded input feature sets (Fig. 15). For each feature set, an artificial neural network (ANN) was trained in 30 independent runs. Predictive performance was assessed using the mean squared error (MSE), mean absolute error (MAE), and coefficient of determination (R^2). For each metric, the mean and standard deviation across the 30 runs were calculated. This comparison allows the collective predictive contribution of concrete composition to be assessed, as the predictive information provided by individual, interdependent features may overlap and therefore not be fully reflected in their individual importance values.

The comparison of different input feature sets showed that using the compressive stress levels alone resulted in poor predictive performance (Fig. 14). Adding concrete age substantially improved the predictions, while the inclusion of all composition-related features further improved the overall performance, although to a lesser extent (Fig. 15). These results indicate that concrete composition provides additional predictive information beyond compressive stress level and concrete age. However, the contribution of concrete age should be interpreted cautiously, as the concrete compositions were tested sequentially and were not represented across the full concrete age range. Consequently, concrete age may partly reflect differences between test campaigns or concrete compositions, and its contribution cannot be fully separated from that of concrete composition.

To further assess the predictive capability of the developed models, the two concrete compositions excluded from the original analysis were used for validation (Fig. 16). Following each training run, the fatigue lives of the two validation concrete compositions were predicted using their respective composition features, concrete age, and applied stress levels as input features. These two compositions were completely excluded from the model development and were therefore unknown to the models during both training and hyperparameter optimization. This procedure provided an independent assessment of the model performance for concrete compositions not represented in the training dataset. For each validation concrete, 30 fatigue-life predictions were performed using the neural network models obtained after hyperparameter optimization. Neural networks were selected for this validation because they achieved the lowest MSE and MAE values for the test data among the evaluated machine learning approaches.

The MSE, MAE, and R^2 results highlight the importance of validating the models using entirely unseen concrete compositions, as a noticeable reduction in predictive performance was observed (Fig. 16). Nevertheless, the models still achieved a reasonable level of predictive accuracy.

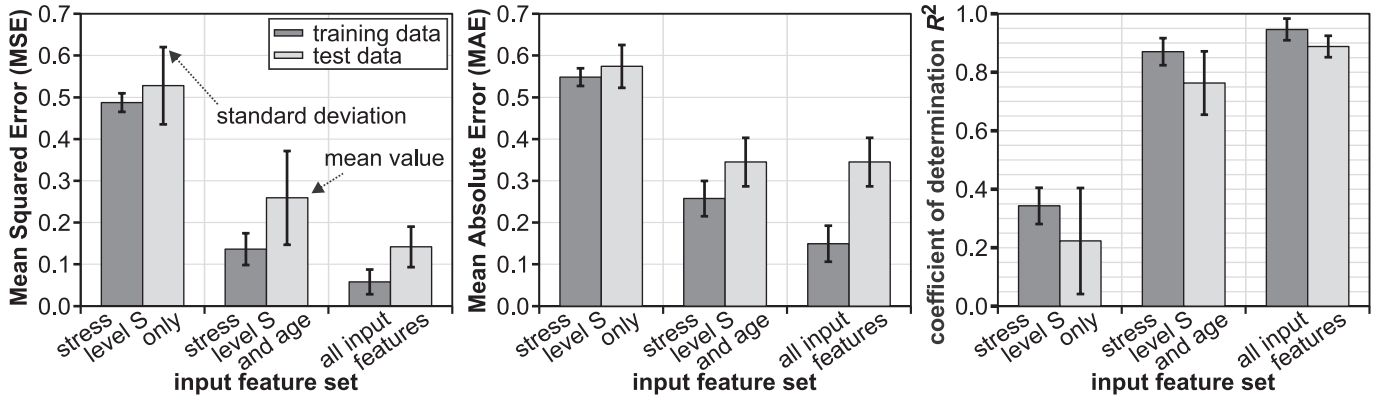

Fig. 15. Comparison of the mean squared error (MSE, left), mean absolute error (MAE, center), and coefficient of determination (R^2, right) for the training and test datasets across different input feature sets, based on 30 independent training runs using the ANN model (graphic: Sören Voß).

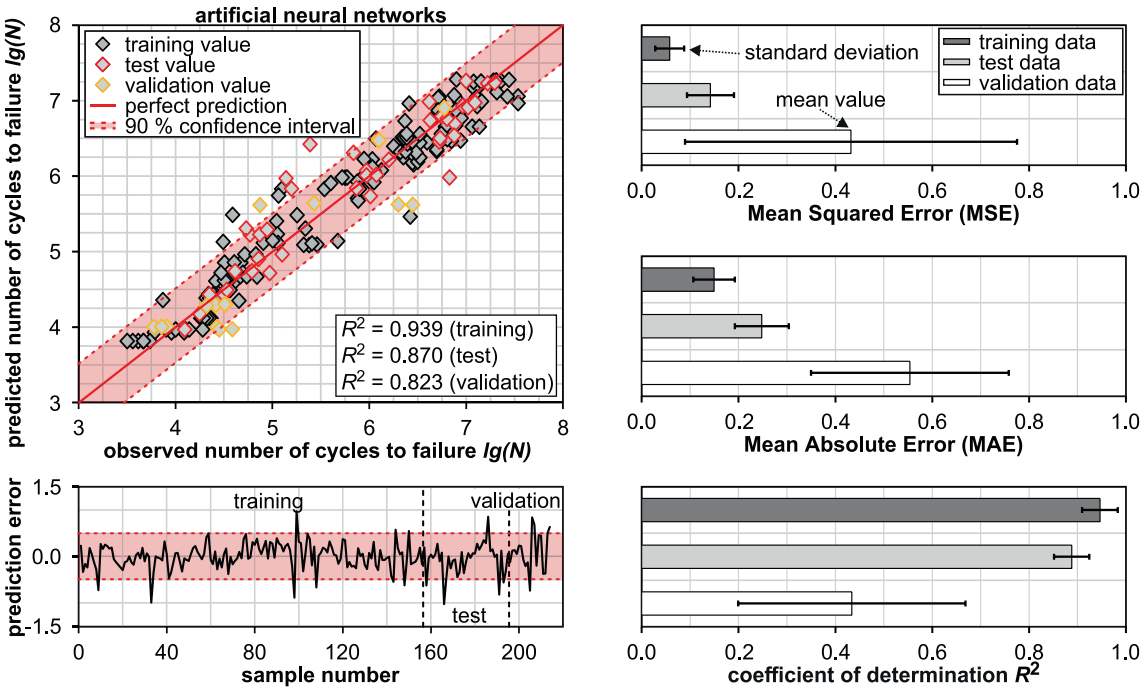

Fig. 16. Comparison of predicted and experimentally determined fatigue lives using artificial neural networks (left), including MSE, MAE, and R^2 values from 30 independent training runs (right; graphic: Sören Voß).

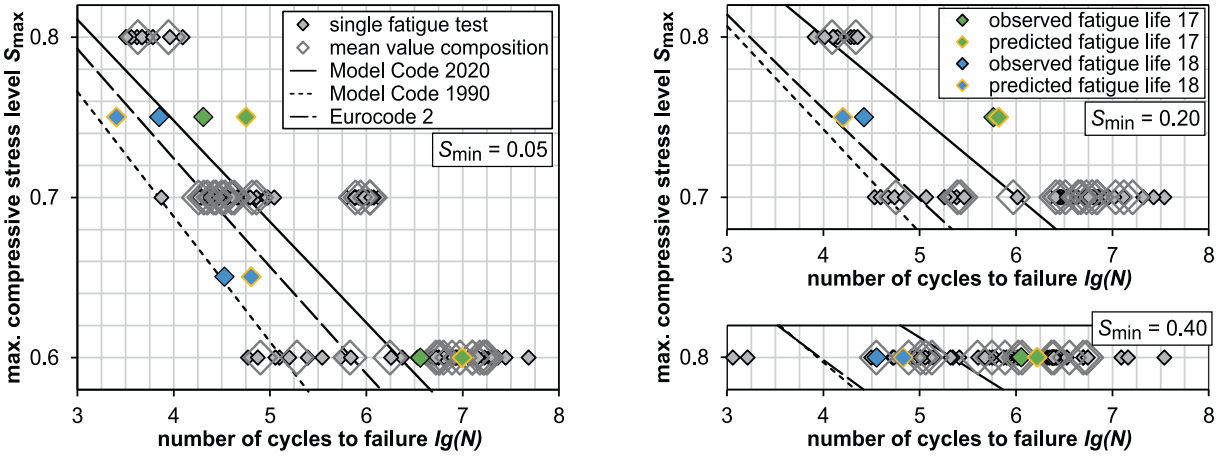

Fig. 17. Summary of fatigue test results, including predicted and experimentally determined fatigue lives of the validation concretes (graphic: Sören Voß).

Following each training run, the fatigue life was predicted for each stress level investigated for the respective validation concrete. The mean of the 30 individual predictions of the logarithmic fatigue life was calculated for each validation concrete and is presented in Fig. 17. To assess the prediction quality, the mean predicted fatigue life was compared with the experimentally determined number of cycles to failure.

Overall, good agreement between the predicted and experimentally determined fatigue lives was obtained (Fig. 17). In particular, the concrete with comparatively shorter experimentally determined fatigue lives was also predicted to exhibit shorter fatigue lives, whereas the concrete with comparatively longer experimental fatigue lives was predicted to exhibit longer fatigue lives. In addition, the validation concretes were tested at some stress levels that were not represented in the database used for model development. However, these stress levels were within the range of the stress levels represented in the database, allowing the predictions to be obtained through interpolation rather than extrapolation. The results therefore indicate that fatigue life can be predicted based on concrete composition for concrete compositions within the parameter range represented in the underlying database, even when the respective composition was not included in the model development.

6. Discussion and summary

A total of 241 fatigue tests under cyclic compressive loading were conducted on small-scale concrete specimens representing 18 high-strength concrete compositions. The resulting data were compiled into a database and systematically analyzed. First, the data were pre-processed and evaluated to ensure their suitability for the subsequent analyses. The main focus was then placed on investigating the influence of concrete composition on fatigue life, with correlation analyses used to identify relevant relationships between composition parameters and fatigue life. Subsequently, machine learning methods were employed to predict fatigue life based on the investigated features. In addition, the influence of specimen temperature on fatigue life was investigated.

The results demonstrate that concrete composition has a measurable

influence on fatigue life. However, the observed relationships cannot generally be attributed to individual composition variables in isolation. This is an important aspect when interpreting the correlation results, as concrete compositions are subject to compositional constraints. An increase in one constituent is typically accompanied by changes in one or more other constituents. Consequently, the correlations observed for individual composition variables may reflect both their direct influence and their relationship with other composition variables. The results further indicate that aggregate type and aggregate size affect fatigue life. In particular, the use of granodiorite and anorthosite was associated with lower normalized fatigue lives, whereas limestone as coarse aggregate and a higher proportion of 8/16 aggregate were associated with higher fatigue lives. These findings are broadly consistent with previous studies emphasizing the role of aggregate stiffness and the resulting heterogeneity of the concrete microstructure [16–21].

Existing *S–N* relationships in Model Code 1990/2020 [8,9] and Eurocode 2 [10] do not explicitly account for concrete composition. The present results indicate that concretes with different compositions but comparable compressive strengths may exhibit substantially different fatigue lives, even when tested under comparable conditions. Consequently, a composition-independent fatigue relationship may lead to different levels of conservatism depending on the concrete composition considered. However, the results do not provide a sufficient basis for directly modifying the partial safety factors specified in current design regulations. The correlations are based on a limited range of high-strength concrete compositions and should therefore be regarded as an indication of composition-dependent fatigue behavior rather than as a direct basis for revised design values. A larger database covering a broader range of concrete compositions and systematically controlled composition parameters would be required to derive composition-dependent design provisions. Such an approach could, in the future, enable fatigue design to be based on the specific concrete composition rather than solely on compressive strength, potentially allowing the composition-independent design provisions currently used to be replaced by more efficient and material-specific approaches.

The machine learning results demonstrate that the number of cycles to failure can be predicted with reasonable accuracy using a combination of concrete composition and compressive stress level. However, the developed approach cannot be reliably transferred to substantially different concrete compositions. Accurate predictions require comparable concrete compositions to be represented in the underlying database. The ML-based approach is therefore well suited for predicting fatigue life for minor variations of previously investigated concrete compositions. For broader applicability, however, the database would need to be substantially expanded to cover a wider range of concrete compositions and material parameters. The strong performance of the ensemble-based model and artificial neural networks indicates that nonlinear relationships between the input features and fatigue life can be captured more effectively than with the linear regression model. The comparatively poor performance of the linear model further suggests that the relationship between concrete composition, compressive stress level, and fatigue life cannot be adequately represented by a purely linear relationship. Nevertheless, the prediction accuracy should not be interpreted as evidence that the models can replace experimental fatigue testing for arbitrary concrete compositions. The database comprises 18 high-strength concrete compositions, and the reliability of predictions outside the range of the training data remains uncertain. The models should therefore primarily be regarded as data-driven tools for identifying relevant composition features and predicting fatigue life within the range represented by the database.

The transferability of the results to real structural components is subject to uncertainties arising from the size effect, differences in loading frequency, and stress redistribution in structural components subjected to bending, among other factors. Nevertheless, the present tests provide a basis for assessing the relative suitability of different concrete compositions for fatigue loading. However, direct extrapolation of the measured fatigue lives to real structural components is not possible without further investigation.

Overall, the results highlight the relevance of concrete composition for fatigue life and demonstrate the potential of machine learning for data-driven fatigue life prediction. The main conclusions of this study are summarized as follows:

- For the high-strength concretes investigated in this study, the *S-N* curves of Model Code 1990 underestimated the fatigue life. The *S-N* curves in Model Code 2020, however, provide a more accurate representation.
- The temperature change was significantly influenced by stress level range and test duration. Higher specimen temperatures result in lower number of cycles to failure.
- The number of cycles to failure showed no significant correlation with mean compressive strength, bulk density, or specimen preparation, but was positively associated with specimen age.
- The number of cycles to failure was associated with the concrete composition. Higher fatigue life was associated with a higher proportion of limestone aggregate, a higher proportion of coarse aggregate (8/16), and a higher equivalent water-to-cement ratio. Conversely, higher cement and binder contents and the use of granodiorite and anorthosite as coarse aggregates were associated with lower fatigue life. These relationships represent statistical associations and should not be interpreted as independent causal effects, as the concrete composition components are interdependent.
- With the compiled dataset, it was possible to predict the number of cycles to failure using machine learning methods. The main advantage was the ability to generate realistic predictions about the experimentally numbers of cycles to failure based on previous fatigue tests. This enables the fatigue life of concrete to be predicted for concrete compositions within the range represented in the database.
- Concrete age was identified as an important predictor of the number of cycles to failure in the machine learning models, in addition to the applied compressive stress levels. However, its independent contribution could not be distinguished from composition-related effects because different concrete compositions were tested at different ages. Nevertheless, concrete age should be considered in fatigue-life prediction, as its influence may be relevant, particularly during prolonged fatigue tests.
- Artificial neural networks and ensemble-based methods, combined with Bayesian hyperparameter optimization, yielded the best predictive performance for the number of cycles to failure. Their superior performance may be related to their ability to capture complex and potentially nonlinear relationships between the input features and fatigue life.

Several limitations should be considered when interpreting the results. The predictive accuracy of the machine learning models depends strongly on the quality and size of the database and the range of parameters represented. The present database is restricted to high-strength concrete and comprises 18 different concrete compositions. The results therefore cannot be directly generalized to normal-strength or ultra-high-strength concrete. Furthermore, the fatigue tests were conducted under specific loading and environmental conditions, and the influence of parameters such as loading frequency, stress ratio, and temperature requires further investigation. In addition, the number of cycles to failure was estimated for tests terminated at predefined run-out levels. Although the estimation procedure is based on strain development and has previously been applied to other concrete types [58,59], the associated uncertainty should be considered when interpreting the statistical and machine learning results.

Further expansion of the database is essential to improve the predictive capability and general applicability of the machine learning models. Additional fatigue tests are currently being conducted using new concrete compositions to expand the parameter space and fill

existing gaps in the database. Systematically varying individual composition parameters would further facilitate the separation of their respective effects on fatigue life. Moreover, incorporating data from normal-strength and ultra-high-strength concretes would extend the range of applicability beyond the high-strength concretes considered in the present study. The resulting expansion of the database is expected to improve the predictive capability of the models and provide a more comprehensive basis for composition-dependent fatigue life prediction and, ultimately, improved fatigue design approaches.

CRediT authorship contribution statement

Sören Voß: Writing – review & editing, Writing – original draft, Visualization, Validation, Software, Methodology, Investigation, Formal analysis, Data curation, Conceptualization. **Silke Scheerer:** Writing – review & editing, Writing – original draft, Investigation. **Raúl Enrique Beltrán Gutiérrez:** Writing – review & editing, Data curation, Conceptualization. **Thorsten Betz:** Writing – review & editing, Project administration, Data curation. **Chongjie Kang:** Writing – review & editing, Validation, Supervision, Project administration. **Steffen Marx:** Supervision, Resources, Project administration, Funding acquisition, Conceptualization.

Declaration of Generative AI and AI-assisted technologies in the writing process

During the preparation of this work, the author(s) used ChatGPT (OpenAI) solely for language improvement, including enhancing clarity and conciseness. The author(s) critically reviewed and revised all AI-assisted suggestions and take full responsibility for the content of the publication.

Declaration of competing interest

The authors declare that they have no known competing financial interests or personal relationships that could have appeared to influence the work reported in this paper.

Acknowledgments

This research was funded by the German Research Foundation (German: Deutsche Forschungsgemeinschaft; short: DFG) in the funding program (grant no. 571276042) *Stochastic evaluation of the fatigue safety of concrete subjected to compressive fatigue loading* (German: Stochastische Bewertung der Ermüdungssicherheit von druckschwellbeanspruchtem Beton). The authors would like to thank the DFG for supporting the research project. We also would like to gratefully acknowledge the support of the colleagues at the Institute of Concrete Construction at Leibniz University Hannover and the Otto Mohr Laboratory at TU Dresden, where the experimental investigations were conducted. We sincerely thank them for their valuable assistance and support throughout the experimental program.

Appendix

Details of the number of fatigue tests by stress level, including concrete age:

Table 5
Number of fatigue tests by stress level, including concrete age.

Concrete composition	Stress level S_{min}/S_{max}	Number of specimens tested	Number of specimens failed	Number of outliers	Mean concrete age at fatigue failure
1	0.05/0.60	3	0	1	118 days
	0.05/0.70	3	3	0	
	0.05/0.80	3	3	0	
	0.20/0.70	3	0	1	
	0.20/0.80	3	3	0	
	0.40/0.80	3	0	1	
2	0.05/0.60	3	3	0	228 days
	0.05/0.70	6	6	0	
	0.05/0.80	6	6	0	
	0.20/0.70	3	3	0	
	0.20/0.80	6	6	0	
	0.40/0.80	3	3	0	
3	0.05/0.60	3	0	0	228 days
	0.05/0.70	3	3	0	
	0.20/0.70	3	0	1	
	0.40/0.80	3	0	0	
4	0.05/0.60	3	0	1	171 days
	0.05/0.70	3	3	1	
	0.20/0.70	3	0	0	
	0.40/0.80	3	0	0	
5	0.05/0.60	3	0	0	179 days
	0.05/0.70	3	3	0	
	0.20/0.70	3	0	1	
	0.40/0.80	3	1	0	
6	0.05/0.60	3	2	0	195 days
	0.05/0.70	3	3	0	
	0.20/0.70	3	1	1	
	0.40/0.80	3	1	1	
7	0.05/0.60	3	0	1	226 days
	0.05/0.70	4	4	0	
	0.20/0.70	3	0	0	
	0.40/0.80	3	2	3	

(*continued on next page*)

Table 5 (*continued*)

Concrete composition	Stress level S_{min}/S_{max}	Number of specimens tested	Number of specimens failed	Number of outliers	Mean concrete age at fatigue failure
8	0.05/0.60	3	3	0	219 days
	0.05/0.70	3	3	1	
	0.20/0.70	3	2	0	
	0.40/0.80	3	3	0	
9	0.05/0.60	3	0	1	165 days
	0.05/0.70	3	3	0	
	0.20/0.70	3	0	1	
	0.40/0.80	3	2	0	
10	0.05/0.60	3	0	1	373 days
	0.05/0.70	3	0	1	
	0.20/0.70	3	0	0	
	0.40/0.80	3	0	1	
11	0.05/0.60	3	0	0	386 days
	0.05/0.70	3	0	0	
	0.20/0.70	3	0	0	
	0.40/0.80	9	2	2	
12	0.05/0.60	3	0	1	134 days
	0.05/0.70	3	3	1	
	0.20/0.70	3	2	0	
	0.40/0.80	3	3	0	
13	0.05/0.60	3	3	0	116 days
	0.05/0.70	3	3	1	
	0.20/0.70	3	3	0	
	0.40/0.80	3	3	1	
14	0.05/0.60	3	0	0	110 days
	0.05/0.70	3	3	0	
	0.20/0.70	3	0	0	
	0.40/0.80	3	3	0	
15	0.05/0.60	3	0	0	296 days
	0.05/0.70	3	0	0	
	0.20/0.70	3	0	0	
	0.40/0.80	3	0	0	
16	0.05/0.60	3	0	0	322 days
	0.05/0.70	3	0	0	
	0.20/0.70	3	0	0	
	0.40/0.80	3	0	0	
17	0.05/0.60	3	0	0	94 days
	0.05/0.75	4	4	1	
	0.20/0.75	4	2	0	
	0.40/0.80	3	0	1	
18	0.05/0.65	3	3	1	152 days
	0.05/0.75	3	3	0	
	0.20/0.75	3	3	1	
	0.40/0.80	3	3	1	

Predefined run-out level:

Table 6
Run-out levels as a function of compressive stress level.

S_{min}/S_{max}	0.05/0.60	0.05/0.65	0.05/0.70	0.05/0.75	0.20/0.70	0.20/0.75	0.40/0.80
Run-out level N_{Stop}	3,000,000	2,000,000	200,000	200,000	2,000,000	2,000,000	500,000

Summary of normalized features for each concrete composition:

Table 7
Summary of normalized features for each concrete composition.

Feature	Concrete composition																	
	1	2	3	4	5	6	7	8	9	10	11	12	13	14	15	16	17*	18*
Normalized cement content	-1.25	-0.28	-0.28	-0.28	-1.25	0.52	-0.71	0.63	-0.28	0.52	-0.71	2.29	1.86	1.65	-0.28	-0.71	0.74	0.63
Normalized blast furnace slag powder content	0.53	0.88	0.88	0.88	0.53	-1.44	0.41	-1.44	0.88	-1.44	0.41	-1.44	-1.44	-1.44	0.76	0.41	1.28	-1.44
Normalized limestone powder content	0.36	-0.19	-0.19	-0.19	1.28	1.28	0.36	1.46	-0.19	1.28	0.36	-2.39	-1.75	-1.38	-0.37	0.36	-2.58	1.46
Normalized binder content	-1.49	0.48	0.48	0.48	-1.49	-0.67	-0.73	-0.50	0.48	-0.67	-0.73	2.25	1.54	1.18	0.35	-0.73	2.59	-0.50
Normalized superplasticizer content	-1.06	1.11	0.18	0.18	-0.44	0.80	-1.06	1.42	1.11	0.80	-1.06	-0.13	-1.43	-1.43	1.11	-0.75	3.90	1.42
Normalized water content	0.48	-1.12	-0.17	-0.17	0.27	0.30	0.72	-1.28	-2.25	0.30	0.72	-0.27	1.59	1.81	-0.44	0.58	-2.50	-1.14
Normalized equivalent w/c ratio	1.66	-0.80	-0.63	-0.63	1.66	0.68	0.68	0.68	-0.63	0.68	0.68	-1.62	-1.62	-0.63	-0.63	0.68	-2.27	0.68
Normalized fines content	-1.68	1.59	0.83	1.29	0.03	-0.29	-0.79	-0.01	1.03	-0.29	-0.79	-0.83	-0.58	-1.17	0.58	-0.32	1.07	0.04
Normalized proportion of limestone	0.83	-1.20	0.83	0.83	0.83	0.83	0.83	-1.20	-1.20	0.83	0.83	-1.20	-1.20	-1.20	0.83	0.83	0.73	-1.20

(*continued on next page*)

Table 7 (*continued*)

Feature	Concrete composition																	
	1	2	3	4	5	6	7	8	9	10	11	12	13	14	15	16	17*	18*
Normalized proportion of granodiorite	-0.37	-0.37	-0.37	-0.37	-0.37	-0.37	-0.37	-0.37	-0.37	-0.37	-0.37	2.93	2.93	0.12	-0.37	-0.37	-0.37	3.05
Normalized proportion of anorthosite	-0.35	-0.35	-0.35	-0.35	-0.35	-0.35	-0.35	2.87	2.87	-0.35	-0.35	-0.35	-0.35	-0.35	-0.35	-0.35	-0.35	-0.35
Normalized proportion of quarz	0.53	0.79	0.53	0.53	0.53	0.53	0.53	-2.25	-2.25	0.53	0.53	-1.19	-0.86	-1.19	0.53	0.53	0.73	0.66
Normalized proportion of 0/1	-0.50	2.11	-0.50	-0.50	-0.50	-0.50	-0.50	-0.50	-0.50	-0.50	-0.50	-0.50	-0.50	1.72	-0.50	-0.50	-0.50	-0.50
Normalized proportion of 0/2	0.57	0.78	0.57	0.57	0.57	0.57	0.57	-1.63	-1.63	0.57	0.57	-1.63	-1.63	-1.63	0.57	0.57	0.72	-1.63
Normalized proportion of 2/8	-0.61	-0.61	-0.61	-0.61	-0.61	-0.61	-0.61	1.57	1.57	-0.61	-0.61	1.67	1.67	1.67	-0.61	-0.61	-0.61	1.57
Normalized proportion of 8/16	-0.42	2.48	-0.42	-0.42	-0.42	-0.42	-0.42	-0.42	-0.42	-0.42	-0.42	-0.23	-0.52	-0.23	-0.42	-0.42	1.13	-0.42
Normalized additional water	0.50	-2.45	0.50	0.50	0.50	0.50	0.50	0.33	0.33	0.50	0.50	-0.02	0.24	-0.02	0.50	0.50	-1.15	0.33
Normalized mean concrete age	-0.04	-0.89	-0.72	-0.72	-0.21	-0.21	0.29	-0.04	-0.89	-0.21	0.29	0.46	2.66	2.32	-1.05	0.13	-3.41	-0.04
Normalized mean S_{min}	-1.08	0.08	0.07	-0.52	-0.49	-0.25	0.30	0.00	-0.74	1.59	1.77	-0.93	-1.08	-1.15	0.79	1.06	-1.31	-0.69
Normalized mean S_{max}	-0.17	-0.23	0.01	0.21	0.01	-0.15	-0.50	0.11	0.10	0.05	0.43	0.21	-0.04	0.03	0.03	0.03	0.07	-0.07
Cement type	0.32	0.47	-0.14	0.00	-0.14	-0.28	-0.45	-0.14	0.00	-0.14	0.20	0.00	-0.28	-0.14	-0.14	-0.14	0.48	0.39
Limestone powder type	0.20	0.20	0.20	-0.53	-0.53	-0.53	-0.53	0.92	0.92	-1.25	-1.25	1.64	1.64	1.64	-1.25	-1.25	-1.25	0.20
Superplasticizer type	0.28	0.28	0.28	0.28	0.28	0.28	0.28	-1.15	-1.15	-1.15	-1.15	1.71	1.71	1.71	-1.15	-1.15	-1.15	3.14

* Indicates the concrete compositions that were used exclusively for validation purposes.

Influence of the concrete temperature on the number of cycles to failure: The concrete temperature was measured at the specimen surface at mid-height during the fatigue tests. Understanding the temperature evolution is important because an increase in concrete temperature reduces its compressive strength and can promote premature fatigue failure [47,79–82]. Fig. 18 shows the temperature change as a function of the number of loading cycles, with one representative fatigue test shown for each compressive stress level. At $S_{min}/S_{max} = 0.40/0.80$, the temperature increase reached a maximum after approximately $\sim 2 \cdot 10^5$ loading cycles, after which no further increase was observed. In contrast, the temperature continuously increased at the other investigated stress levels until failure ($S_{min}/S_{max} = 0.05/0.70$). The specimen tested at $S_{min}/S_{max} = 0.05/0.60$ exhibited a similar initial temperature evolution to the specimen tested at $S_{min}/S_{max} = 0.40/0.80$. However, after reaching an initial maximum followed by a slight decrease, the temperature increased again shortly before failure. This renewed temperature increase coincided with the onset of phase III of fatigue development. During this phase, existing microcracks coalesce into macrocracks, increasing friction between crack surfaces and potentially contributing to further temperature generation [83,84]. In contrast, the test at $S_{min}/S_{max} = 0.40/0.80$ was terminated before phase III was reached, and no subsequent temperature increase was observed. Furthermore, the initial rate of temperature increase was related to the applied stress range. A smaller stress range resulted in a lower initial temperature increase rate. Similar relationships have been reported in previous studies [45].

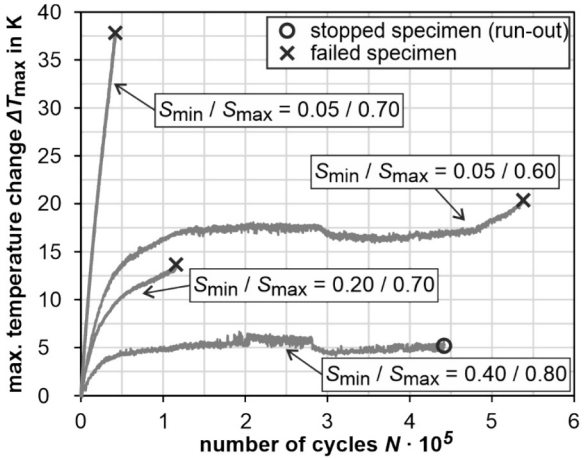

Fig. 18. Exemplary illustration of temperature changes in cyclically loaded concrete specimens at different compressive stress levels (graphic: Sören Voß).

Fig. 19 shows the maximum temperature change during cyclic loading as a function of the number of cycles to failure, separated by compressive stress level. The largest mean temperature changes occurred at compressive stress levels of $S_{min}/S_{max} = 0.05/0.70$ and 0.05/0.60. Notably, the test specimens that failed relatively early exhibited higher temperature changes at $S_{min}/S_{max} = 0.05/0.60$. Conversely, significantly smaller temperature changes were measured at the fatigue tests that achieved high number of cycles to failure. Smaller temperature increases were observed for the remaining compressive stress levels, which can be attributed to shorter test durations and smaller stress level ranges. The smallest temperature changes occurred at $S_{min}/S_{max} = 0.40/0.80$. At this compressive stress level, it can be assumed that the temperature observed increases had no significant negative effect on the number of cycles to failure [85]. At comparable stress levels, specimens with longer fatigue lives exhibited lower maximum temperature rises, except at stress ratios of $S_{min}/S_{max} = 0.05/0.80$ and 0.20/0.80 due to the short test durations. This finding indicates an association between self-heating and fatigue behavior; however, a causal relationship cannot be established, as temperature evolution may also reflect differences in damage development during cyclic loading.

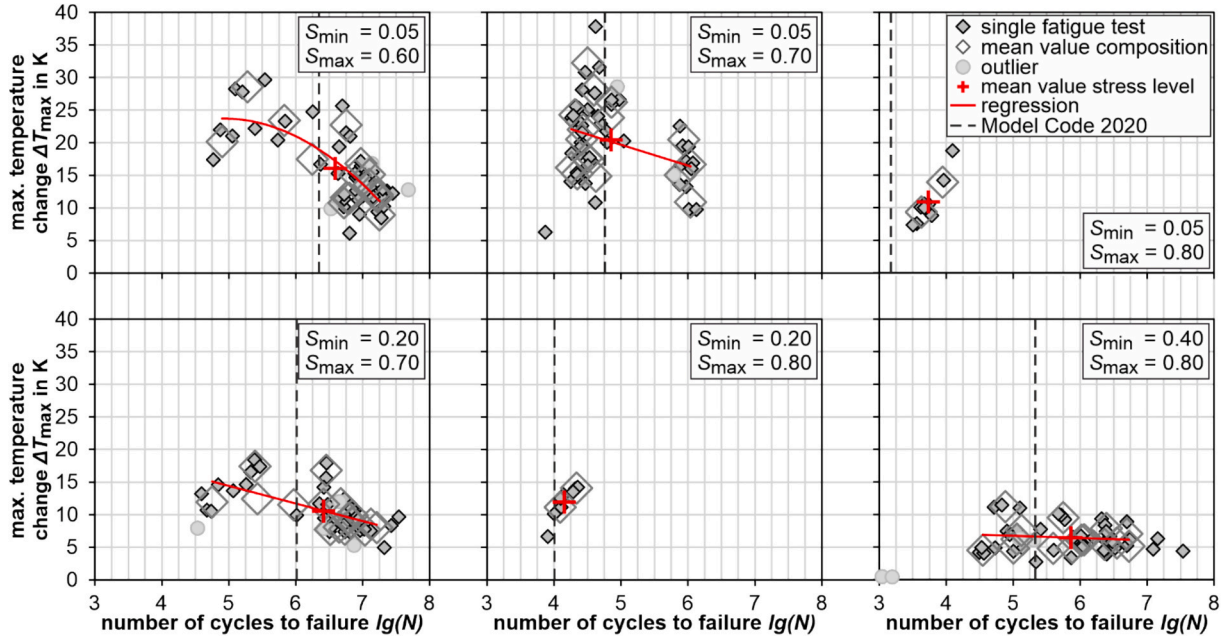

Fig. 19. Maximum temperature changes during fatigue tests, classified by compressive stress level and number of cycles to failure (graphic: Sören Voß).

A comparison of stress level range defined as $S_{max} - S_{min} = \Delta\sigma/f_c$ at different compressive stress levels with the measured maximum temperature changes of Fig. 19 shows a clear correlation between the two parameters (Fig. 20, left). The temperature of all specimens tested at compressive stress levels (S_{min}/S_{max} = 0.05/0.70, 0.05/0.80, and 0.20/0.80) had not yet stabilized (see Fig. 18 for S_{min}/S_{max} = 0.05/0.70 as an example), so these results were excluded from the subsequent regression analysis. In these cases, the maximum temperature change limited the number of cycles to failure. This is why maximum temperature change has a decisive influence on the number of cycles to failure or the time of failure. For tests at compressive stress levels that exhibit stabilized temperature changes prior to fatigue failure or test termination, the maximum temperature change can be compared with the stress level range. Notably, the magnitude of the temperature increase is attributable to the stress level range. In Fig. 20 (right), the maximum temperature change is plotted against the normalized number of cycles to failure for each compressive stress level. It can be seen that a lower normalized number of cycles to failure corresponds to a higher maximum temperature change. The compressive stress levels S_{min}/S_{max} = 0.05/0.70, 0.05/0.80, and 0.20/0.80 are again excluded from this analysis. This result shows that a greater temperature increase negatively affects the number of cycles to failure, see also [46] and [67].

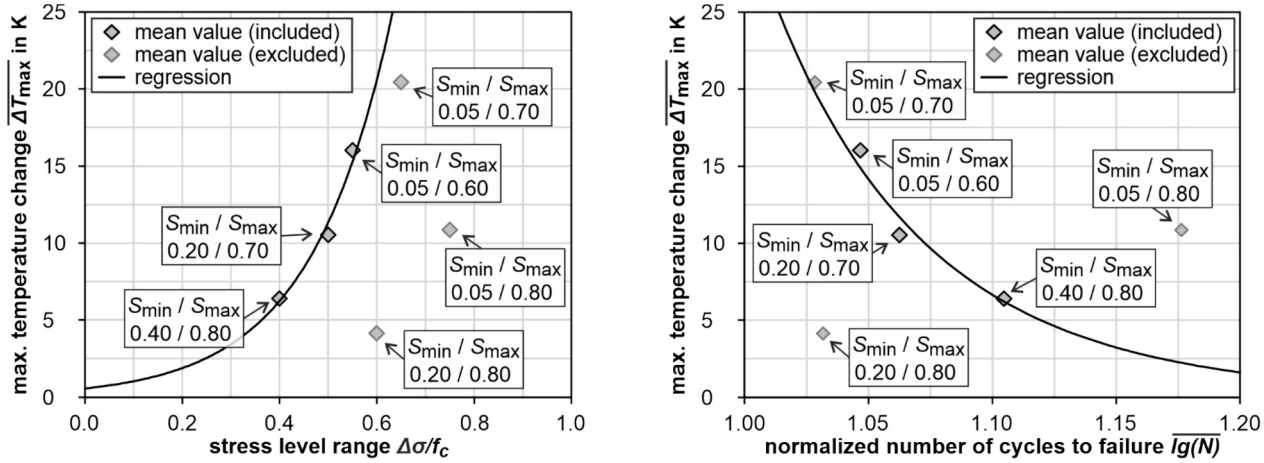

Fig. 20. Comparison of the mean temperature change with the stress level range (left) and with the mean normalized number of cycles to failure (right; graphic: Sören Voß).

Data availability

The authors do not have permission to share data.

References

[1] Fürll F, Klein F, Hartwig S, Kang C, Betz T, Marx S. Experimental and analytical study on the load-bearing capacity of segmented tower structures with dry joints under combined loading. Struct Concr 2024;25:3347–60. https://doi.org/10.1002/suco.202300873.

[2] Hartwig S, Kang C, Fürll F, Klein F, Classen M, Marx S. Development of a new analytical model for circular concrete ring segments with dry joints under

combined effects. Struct Concr 2025;26:3256–68. https://doi.org/10.1002/suco.202400194.
[3] Ziegler L, Gonzalez E, Rubert T, Smolka U, Melero JJ. Lifetime extension of onshore wind turbines: A review covering Germany, Spain, Denmark, and the UK. Renew Sustain Energy Rev 2018;82:1261–71. https://doi.org/10.1016/j.rser.2017.09.100.
[4] Bai X, He M, Ma R, Huang D, Chen J. Modelling fatigue degradation of the compressive zone of concrete in onshore wind turbine foundations. Constr Build Mater 2017;132:425–37. https://doi.org/10.1016/j.conbuildmat.2016.12.026.
[5] Schramm C, Birkner D, Marx S. Resonance-based testing facility for fatigue tests of different axially loaded structural elements. Eng Struct 2024;298:117045. https://doi.org/10.1016/j.engstruct.2023.117045.
[6] Basaldella M, Jentsch M, Oneschkow N, Markert M, Lohaus L. Compressive fatigue investigation on high-strength and ultra-high-strength concrete within the SPP 2020. Materials 2022;15(11):3793. https://doi.org/10.3390/ma15113793.
[7] Dreger D, Oneschkow N. Sequence effects on the strain development of high-strength concrete due to two-stage fatigue loading. Int J Fatigue 2026;212:109756. https://doi.org/10.1016/j.ijfatigue.2026.109756.
[8] CEB – Comité Euro-internationale du Béton (1993) CEB-FIP Model Code 1990. London: Bulletin d'Information no. 213/214, Thomas Telford Ltd; 1993.
[9] Fédération International du Béton (ed.). Lausanne: fib model code for concrete structures 2020; 2023, ISBN 978-2-88394-176-2.
[10] DIN EN 1992-2:2010-12. Eurocode 2: Design of concrete structures—Part 2: Concrete bridges—Design and detailing rules; German version EN 1992-2:2005 + AC:2008. Berlin: German Institute for Standardisation; 2010. https://doi.org/10.31030/1723952.
[11] Schmidt B, Schneider S, Marx S. Betonermüdung – Sicherheiten und entwicklungspotenziale aktueller Nachweiskonzepte. Bautechnik 2019;96(4):329–37. https://doi.org/10.1002/bate.201900003.
[12] Voß S, Schmidt B, Oettel V. Fatigue resistance of concrete: influence of time-dependent scattering of compressive strength. Mater Struct 2025;58:85. https://doi.org/10.1617/s11527-024-02517-5.
[13] Lee MK, Barr BIG. An overview of the fatigue behaviour of plain and fibre reinforced concrete. Cem Concr Compos 2004;26(4):299–305. https://doi.org/10.1016/S0958-9465(02)00139-7.
[14] Comité Euro-International du Béton. Fatigue of concrete structures: State-of-the-art report. Lausanne, Switzerland: CEB: Bulletin d'Information No. 188; 1988.
[15] Kachkouch FZ, Noberto CC, Babadopulos LFAL, Melo ARS, Machado AML, Sebaibi N, et al. Fatigue behavior of concrete: a literature review on the main relevant parameters. Constr Build Mater 2022;338:127510. https://doi.org/10.1016/j.conbuildmat.2022.127510.
[16] Oneschkow N, Timmermann T. Influence of the composition of high-strength concrete and mortar on the compressive fatigue behaviour. Mater Struct 2022;55:83. https://doi.org/10.1617/s11527-021-01868-7.
[17] Scheiden T, Oneschkow N. Influence of coarse aggregate type on the damage mechanism in high-strength concrete under compressive fatigue loading. Struct Concr 2019;20:1212–9. https://doi.org/10.1002/suco.201900029.
[18] Timmermann T, Löhnert S, Oneschkow N. Composition Influenced Damage Development in High-strength Concrete due to Cyclic Loading. In: Oneschkow N, Lohaus L, editors. Springer: Cyclic Deterioration of High-Performance Concrete – Reports of the SPP 2020 Experimental-Virtual-Lab, chapter 3; 2008. p. 31–49. https://doi.org/10.1007/978-3-032-19394-0_3.
[19] Breitenbücher R, Ibuk H, Yüceoglu S. Beeinflusst die Kornsteifigkeit der Gesteinskörnung im Beton den Degradationsprozess infolge zyklischer Druckbeanspruchung? Beton- Stahlbetonbau 2008;103(5):318–23. https://doi.org/10.1002/best.200800615.
[20] Dubey S, Kumar B, Ray S. Heterogeneity induced fracture characterization of concrete under fatigue loading using digital image correlation and acoustic emission techniques. Int J Fatigue 2024;188:108474. https://doi.org/10.1016/j.ijfatigue.2024.108474.
[21] Oneschkow N, Timmermann T. Löhnert S (2022) Compressive fatigue behaviour of high-strength concrete and mortar: experimental investigations and computational modelling. Materials. 2022;15(1):319. https://doi.org/10.3390/ma15010319.
[22] Li LJ, Xu LH, Huang L, Xu FD, Huang YL, Cui K, et al. Compressive fatigue behaviors of ultra-high performance concrete containing coarse aggregate. Cem Concr Compos 2022;128:104425. https://doi.org/10.1016/j.cemconcomp.2022.104425.
[23] Skarzynski L, Marzec I, Tejchman J. Fracture evolution in concrete compressive fatigue experiments based on X-ray micro-CT images. Int J Fatigue 2019;122:256–72. https://doi.org/10.1016/j.ijfatigue.2019.02.002.
[24] Becks H, Classen M. Influence of coarse aggregates on the fatigue behavior of high-strength concrete under mode II loading. Constr Build Mater 2025;491:142565. https://doi.org/10.1016/j.conbuildmat.2025.142565.
[25] Hordijk DA, Wolsink GM, de Vries J. Fracture and fatigue behaviour of a high strength limestone concrete compared to gravel concrete. HERON 1995;40(2):128–45.
[26] Yan H, Sun W, Chen H. The effect of silica fume and steel fiber on the dynamic mechanical performance of high strength concrete. Cem Concr Res 1999;29(3):423–6. https://doi.org/10.1016/S0008-8846(98)00235-X.
[27] Tan H, Yuan P, Sun D, Fan X, Wang C, Liu J. Ratio of water to cement and supplementary cementitious materials on mechanical and impact resistance properties of reactive powder concrete. Sci Rep 2025;15:7480. https://doi.org/10.1038/s41598-025-92097-3.
[28] Vicente MA, González DC, Mínguez J, Tarifa MA, Ruiz G, Hindi R. Influence of the pore morphology of high strength concrete on its fatigue life. Int J Fatigue 2018;112:106–16. https://doi.org/10.1016/j.ijfatigue.2018.03.006.
[29] Ferdiansyah T, Ismy R, Shahzad S, Rafiq W, Nadeem K. The influence of the water–cement ratio on concrete resistivity: a temperature and saturation dependent analysis using an experimental and predictive approach. CivilEng 2025;6(3):38. https://doi.org/10.3390/civileng6030038.
[30] Graf O, Brenner E. Versuche zur Ermittlung der Widerstandsfähigkeit von Beton gegen oftmals wiederholte Druckbeanspruchung, Zweiter Teil. In: Deutscher Ausschuss für Eisenbeton 83. Berlin: Ernst and Sohn; 1936.
[31] Bennett EW, Muir SE. Some fatigue tests of high-strength concrete in axial compression. Mag Concr Res 1967;19(59):113–7. https://doi.org/10.1680/macr.1967.19.59.113.
[32] Kim J-K, Kim Y-Y. Experimental study of the fatigue behavior of high strength concrete. Cem Concr Res 1996;26(10):1513–23. https://doi.org/10.1016/0008-8846(96)00151-2.
[33] Van Leeuwen J, Siemens AJM. Miner's rule with respect to plain concrete. Heron 1979;24(1).
[34] Tue NV, Mucha S. Ermüdungsfestigkeit von hochfestem Beton unter Druckbeanspruchung. Bautechnik 2006;83(7):497–504. https://doi.org/10.1002/bate.200610043.
[35] Hohberg R. Zum Ermüdungsverhalten von Beton [dissertation]. Germany: Technische Universität Berlin; 2004.
[36] Thiele M. Experimentelle Untersuchung und Analyse der Schädigungsevolution in Beton unterhochzyklischen Ermüdungsbeanspruchungen [dissertation]. Berlin, Germany: BAM-Dissertationsreihe 140; 2016.
[37] Petković G, Rosseland S, Stemland H. High Strength Concrete SP3 – Fatigue. Report 3.2: Fatigue of High Strength Concrete. Trondheim, Norway: SINTEF Structural Engineering – FCB; 1992.
[38] Basaldella M, Kern B, Lohaus L, Oneschkow N. Material Properties and Fatigue Resistance of the Reference High-strength and Ultra-high-strength Concrete of SPP 2020. In: Oneschkow N, Lohaus L, editors. Springer: Cyclic Deterioration of High-Performance Concrete – Reports of the SPP 2020 Experimental-Virtual-Lab, chapter 2; 2026. p. 9–30. https://doi.org/10.1007/978-3-032-19394-0_2.
[39] Kono S, Hasegawa H, Mori K, Ichioka Y, Sakashita M, Watanabe F. Low cycle fatigue characteristics of high strength concrete. In: Proceedings of the 8th International Symposium on Utilization of High-Strength and High-Performance Concrete, Tokyo, Japan; 27–29 October 2008. p. 616–21.
[40] Basaldella M, Kern B, Oneschkow N, Lohaus L. Zum festigkeitsabhängigen Ermüdungswiderstand von Beton. Berlin, Germany: Beuth Verlag; 2024.
[41] Schmidt B, Marx S, Schneider S, Betz T. Einfluss der Druckfestigkeitsstreuung auf den Ermüdungswiderstand von druckschwellbeanspruchtem Beton. Beton-Stahlbetonbau 2021;116(8):575–86. https://doi.org/10.1002/best.202100025.
[42] Voß S, Beltrán Gutiérrez RE, Marx S. Influence of the distribution function on the statistical scatter adjustment of the number of cycles to failure of concrete under fatigue. ce/papers 2025;8(3–4):169–76. https://doi.org/10.1002/cepa.3338.
[43] Basaldella M, Oneschkow N, Lohaus L. Influence of the specimen production and preparation on the compressive strength and the fatigue resistance of HPC and UHPC. Mater Struct 2021;54:99. https://doi.org/10.1617/s11527-021-01696-9.
[44] Hümme J, von der Haar C, Lohaus L, Marx S. Fatigue behaviour of a normal-strength concrete – number of cycles to failure and strain development. Struct Concr 2016;4:637–45. https://doi.org/10.1002/suco.201500139.
[45] Deutscher M, Tran NL, Scheerer S. experimental investigations on the temperature increase of ultra-high performance concrete under fatigue loading. Appl Sci 2019;9(19):4087. https://doi.org/10.3390/app9194087.
[46] Baktheer A, Chudoba R. Experimental study of the interacting effects of loading rate and temperature on concrete fatigue behavior under compression. Constr Build Mater 2025;458:139466. https://doi.org/10.1016/j.conbuildmat.2024.139466.
[47] Deutscher M, Markert M, Scheerer S. Influence of temperature on the compressive strength of high performance and ultra-high performance concretes. Struct Concr 2021;23:2381–90. https://doi.org/10.1002/suco.202100153.
[48] Becks H, Classen M. New insights into the load sequence effect: Experimental characterization and incremental modeling of plain high-strength concrete under mode II fatigue loading with variable amplitude. Int J Fatigue 2024;185:108334. https://doi.org/10.1016/j.ijfatigue.2024.108334.
[49] Koschemann M, Curbach M, Marx S. Bond behavior of reinforced high-strength concrete under high-cycle fatigue pull-out loading. Int J Fatigue 2025;198:108944. https://doi.org/10.1016/j.ijfatigue.2025.108944.
[50] Feng D-C, Liu Z-T, Wang X-D, Chen Y, Chang J-Q, Wei D-F, et al. Machine learning-based compressive strength prediction for concrete: An adaptive boosting approach. Constr Build Mater 2020;230:117000. https://doi.org/10.1016/j.conbuildmat.2019.117000.
[51] Paudel S, Pudasaini A, Kumar S, Kharel E. Compressive strength of concrete material using machine learning techniques. Cleaner Eng Technol 2023;15:100661. https://doi.org/10.1016/j.clet.2023.100661.
[52] Abdellatief M, Hassan YM, Elnabwy MT, Wong LS, Chin RJ, Mo KH. Investigation of machine learning models in predicting compressive strength for ultra-high-performance geopolymer concrete: a comparative study. Constr Build Mater 2024;436:136884. https://doi.org/10.1016/j.conbuildmat.2024.136884.
[53] Baktheer A, Aldakheel F. Physics-based machine learning for fatigue lifetime prediction under non-uniform loading scenarios. Comput Methods Appl Mech Eng 2025;444:118116. https://doi.org/10.1016/j.cma.2025.118116.
[54] Elsayed ES, Baktheer A, Aldakheel F. ML-accelerated framework for fatigue life-timescale homogenization and cyclic damage evolution under physics constraints. Int J Numer Meth Eng 2026;127:e70394. https://doi.org/10.1002/nme.70394.
[55] Wu J, Zhang B, Xu J, Jin L, Diao B. Probabilistic fatigue life prediction for RC beams under chloride environment considering the statistical uncertainty by

Bayesian updating. Int J Fatigue 2023;173:107680. https://doi.org/10.1016/j.ijfatigue.2023.107680.
[56] Gao J, Pan R, Yuan Y, Zhou J, Ding H, Kong W. A novel multiaxial fatigue life prediction method based on multi-scale physical neural network. Reliab Eng Syst Saf 2026;269:112049. https://doi.org/10.1016/j.ress.2025.112049.
[57] Sparks PR, Menzies JB. The effect of rate of loading upon the static and fatigue strengths of plain concrete in compression. Mag Concr Res 1973;25(83):73–80. https://doi.org/10.1680/macr.1973.25.83.73.
[58] Voß S, Kang C, Marx S. Strain- and energy-based fatigue life prediction models for high-strength concrete under cyclic compressive loading. Int J Fatigue 2027;215:110010. https://doi.org/10.1016/j.ijfatigue.2026.110010.
[59] Kerkeni W, Baktheer A, Aguilar M, Becks H, Vořechovský M, Classen M, et al. Stable deformation growth as a fatigue life indicator for concrete: Experimental and multiscale numerical insights. Int J Fatigue 2026;214:109883. https://doi.org/10.1016/j.ijfatigue.2026.109883.
[60] Schober P, Boer C, Schwarte LA. Correlation coefficients: appropriate use and interpretation. Anesth Analg 2018;126(5):1763–8. https://doi.org/10.1213/ANE.0000000000002864.
[61] Oneschkow N, Hümme J, Lohaus L. Compressive fatigue behavior of high-strength concrete in dry and wet environment. Constr Build Mater 2020;262:119700. https://doi.org/10.1016/j.conbuildmat.2020.119700.
[62] Schneider S, Hümme J, Marx S, Lohaus L. Untersuchungen zum Einfluss der Probekörpergröße auf den Ermüdungswiderstand von hochfestem Beton. Beton-Stahlbetonbau 2018;113(1):58–67. https://doi.org/10.1002/best.201700051.
[63] Saucedo L, Yu RC, Medeiros A, Zhang X, Ruiz G. A probabilistic fatigue model based on the initial distribution to consider frequency effect in plain and fiber reinforced concrete. Int J Fatigue 2013;48:308–18. https://doi.org/10.1016/j.ijfatigue.2012.11.013.
[64] Medeiros A, Zhang X, Ruiz G, de Souza Lima Velasco M. Effect of the loading frequency on the compressive fatigue behavior of plain and fiber reinforced concrete. Int J Fatigue 2015;70:342–50. https://doi.org/10.1016/j.ijfatigue.2014.08.005.
[65] Holmen JO. Fatigue of concrete by constant and variable amplitude loading [dissertation]. Norway: University of Trondheim; 1979.
[66] Klausen D. Festigkeit und Schädigung von Beton bei häufig wiederholter Beanspruchung [dissertation]. Germany: Technische Hochschule Darmstadt; 1978.
[67] von der Haar C, Marx S. A strain model for fatigue-loaded concrete. Struct Concr 2017;19:463–71. https://doi.org/10.1002/suco.201700029.
[68] Birkner D, Beltrán Gutiérrez RE, Marx S. Comparison of stiffness degradation in fatigue-loaded concrete cylinders and large-scale beams. Eng Struct 2024;302:117360. https://doi.org/10.1016/j.engstruct.2023.117360.
[69] Grünberg J, Lohaus L, Ertel C, Elsmeier K. Ermüdung von UHPC unter ein- und mehraxialer Beanspruchung - Experimentelle Untersuchung und Entwicklung eines mechanischen Modells. In: Schmidt M, Fehling E, Fröhlich S, Thiemicke J, editors. Nachhaltiges Bauen mit ultra-hochfestem Beton (UHPC). Kassel: Kassel University Press GmbH; 2014. p. 453–78.
[70] Wefer M. Materialverhalten und Bemessungswerte von ultrahochfestem Beton unter einaxialer Ermüdungsbeanspruchung [dissertation]. In: Report of the Institute of Building Materials Science (7). Germany: Leibniz Universität Hannover; 2010.
[71] Oneschkow N. Fatigue behaviour of high-strength concrete with respect to strain and stiffness. Int J Fatigue 2016;87:38–49. https://doi.org/10.1016/j.ijfatigue.2016.01.008.
[72] Deutscher M, Tran NL, Scheerer S. Experimental investigation of load-induced temperature development in UHPC subjected to cyclic loading. In: Derkowski W, Gwoździewicz P, Fernández Ordóñez D, Hojdys Ł, Kwiecień K, editors. Concrete – Innovations in Materials, Design and Structures. Kraków, Poland: Proceedings of the fib Symposium 2019; 27–29 May 2019. p. 1873–80.
[73] DIN Deutsches Institut für Normung e. V.. Testing hardened concrete - Part 1: Shape, dimensions and other requirements for specimens and moulds; German version EN 12390-1:2021. In: Berlin: German Institute for Standardisation; 2021. https://doi.org/10.31030/3240228.
[74] Węglarczyk S. Kernel density estimation and its application. ITM Web of Conferences 2018;23:00037. https://doi.org/10.1051/itmconf/20182300037.
[75] Varoquaux G, Colliot O. Evaluating Machine Learning Models and Their Diagnostic Value. In: Colliot O, editor. Machine Learning for Brain Disorders. Neuromethods 197. New York: Humana Press; 2023. https://doi.org/10.1007/978-1-0716-3195-9_20.
[76] Drogkoula M, Kokkinos K, Samaras N. A Comprehensive Survey of Machine Learning Methodologies with Emphasis in Water Resources Management. App Sci 2023;13(22):12147. https://doi.org/10.3390/app132212147.
[77] Wu J, Chen X-Y, Zhang H, Xiong L-D, Lei H, Deng S-H. Hyperparameter optimization for machine learning models based on Bayesian optimization. J Electron Sci Technol 2019;17(1):26–40. https://doi.org/10.11989/JEST.1674-862X.80904120.
[78] Robnik-Šikonja M, Kononenko I. Theoretical and empirical analysis of ReliefF and RReliefF. Mach Learn 2003;53:23–69.
[79] Omar Tanash A, Abu Bakar BH, Muthusamy K, Al Biajawi MI. Effect of elevated temperature on mechanical properties of normal strength concrete: an overview. Mater Today Proc 2023;107:152–7. https://doi.org/10.1016/j.matpr.2023.09.053.
[80] Nigussie T, Raj SJ, Kumar MV. The influence of elevated temperature on the strength of concrete. AIP Conf Proc 2023;2766:020051. https://doi.org/10.1063/5.0146188.
[81] Salah HB, Hani M. An investigation of the effect of high temperature on the strength compression and ultrasonic pulse velocity of self-compacting concrete. J Eng Exact Sci 2024;10(1):16818. https://doi.org/10.18540/jcecvl10iss1pp16818.
[82] Bode M, Marx S. Energetic damage analysis regarding the fatigue of concrete. Struct Concr 2020;22(Suppl. 1):E851–9. https://doi.org/10.1002/suco.202000416.
[83] Bode M, Marx S. Heat Generation during Fatigue Tests on Concrete Specimens. In: Derkowski W, Gwoździewicz P, Fernández Ordóñez D, Hojdys Ł, Kwiecień K, editors. Concrete – Innovations in Materials, Design and Structures. Kraków, Poland: Proceedings of the fib Symposium 2019; 27–29 May 2019. p. 1881–7.
[84] Bode M. Energetische Schädigungsanalyse von ermüdungsbeanspruchtem Beton [dissertation]. Report of the Institute of concrete constructions (17). Germany: Leibniz Universität Hannover; 2020.
[85] Schneider S. Frequenzabhängigkeit des Ermüdungswiderstands von hochfestem Beton [dissertation]. Germany: Leibniz Universität Hannover; 2021.